Available online at www.sciencedirect.com
SCIENCE DIRECT
Earth and Planetary Science Letters 240 (2005) 122–148
EPSL
www.elsevier.com/locate/epsl

Geochemical modeling of evaporation processes on Mars: Insight from the sedimentary record at Meridiani Planum

N.J. Tosca [a,*], S.M. McLennan [a], B.C. Clark [b], J.P. Grotzinger [c], J.A. Hurowitz [a], A.H. Knoll [d], C. Schröder [e], S.W. Squyres [f]

[a] *Department of Geosciences, State University of New York, Stony Brook, NY 11794, USA*
[b] *Lockheed Martin Corporation, Littleton, CO 80127, USA*
[c] *Earth, Atmos. and Planetary Sci., Massachusetts Institute of Technology, Cambridge, MA 02139, USA*
[d] *Botanical Museum, Harvard University, Cambridge, MA 02138, USA*
[e] *Institut für Anorganische und Analytische Chemie, Johannes Gutenberg-Universität, Mainz, Germany*
[f] *Department of Astronomy, Cornell University, Ithaca, NY 14853, USA*

Accepted 22 September 2005
Available online 2 November 2005
Editor: A.N. Halliday

Abstract

New data returned from the Mars Exploration Rover (MER) mission have revealed abundant evaporites in the sedimentary record at Meridiani Planum. A working hypothesis for Meridiani evaporite formation involves the evaporation of fluids derived from the weathering of martian basalt and subsequent diagenesis. On Earth, evaporite formation in exclusively basaltic settings is rare. However, models of the evaporation of fluids derived from experimentally weathering synthetic martian basalt provide insight into possible formation mechanisms. The thermodynamic database assembled for this investigation includes both Fe^{2+} and Fe^{3+} in Pitzer's ion interaction equations to evaluate Fe redox disequilibrium at Meridiani Planum. Modeling results suggest that evaporation of acidic fluids derived from weathering olivine-bearing basalt should produce Mg, Ca, and Fe-sulfates such as jarosite and melanterite. Calculations that model diagenesis by fluid recharge predict the eventual breakdown of jarosite to goethite as well as the preservation of much of the initial soluble evaporite component at modeled porosity values appropriate for relevant depositional environments (<0.30). While only one of several possible formation scenarios, this simple model is consistent with much of the chemical and mineralogical data obtained on Meridiani Planum outcrop.

Keywords: Mars; Mars exploration rovers; Geochemistry; Evaporites; Weathering; Sulfates

1. Introduction

The *Opportunity* rover's analysis of an impure evaporite component present in the martian sedimentary record has revealed an unusual geochemical system. The rich data set returned by the rover during its primary and extended mission phases show that this system is complex, involving periods of evaporation and subsequent diagenesis [1]. The recent characterization of sedimentary rocks several meters thick inside "Endurance" crater, as well as independent spectral and geomorphologic evidence, suggests that evaporites are not limited to the very surface, but occur through a

* Corresponding author. Department of Geosciences, State University of New York, Stony Brook, NY 11794-2100, USA. Tel.: +1 631 632 1936; fax: +1 631 632 8240.
E-mail address: ntosca@ic.sunysb.edu (N.J. Tosca).

0012-821X/$ - see front matter © 2005 Elsevier B.V. All rights reserved.
doi:10.1016/j.epsl.2005.09.042

substantial stratigraphic interval over a wide expanse of the martian surface [2,3]. As a result, fluid evaporation appears to have played a more important role in the martian geologic past than previously thought.

Evaporite mineral assemblages are among the best recorders of paleo-fluid chemistry (see [4]) and an understanding of evaporite geochemistry at Meridiani will place important constraints on the chemistry of ancient aqueous fluids. However, the evaporation of fluids derived exclusively from basaltic weathering is a rare process on Earth and there are few terrestrial environments which can be studied as analogs [5,6]. Also, because of the complex physical and chemical nature of the sedimentary rocks at Meridiani Planum, the fluid chemistry prior to evaporation is difficult to derive by inverse modeling. An alternative approach is taken here to investigate mineral precipitation during the evaporation of typical basaltic weathering-derived fluids. Data obtained in the laboratory from the weathering of synthetic martian basalt provide a starting point for the investigation of evaporation processes at Meridiani Planum.

Advances in accurately predicting the sequence of mineral precipitation from evaporating solutions allow for an in depth understanding of evaporite geochemistry in many terrestrial environments [7]. The most common approach to modeling evaporative processes is to employ Pitzer's ion interaction equations, which allow for the calculation of mineral solubility in electrolyte solutions of high ionic strength [7–9]. Based on sound thermodynamic principles and robust datasets, this approach has been successfully applied to a range of geologic problems. The chemical and mineralogical characteristics of the outcrop observed at Meridiani, however, show that adequate modeling of this geochemical system requires that additional components be added to current thermodynamic models, namely Fe^{2+} and Fe^{3+}. Both Fe^{2+} and Fe^{3+} must be added because Fe-sulfates appear to have played an important role in evaporite geochemistry on Mars, and Fe redox disequilibrium is the rule, not the exception in many aqueous environments on Earth [10]. Consequently, some degree of disequilibrium between Fe(II) (a roman numeral will be used to denote all possible aqueous species) and atmospheric oxygen is expected in the Meridiani geochemical system, especially under acidic conditions where Fe oxidation is sluggish. While the available data for adding Fe^{2+} into such models have improved in recent years [11,12], the expansion of datasets to include Fe^{3+} remains problematic, because few experimental data are available to derive various input parameters and test resulting models. The goals of this paper, therefore, are to: (1) develop a thermodynamic dataset suitable for modeling evaporation in the Meridiani system and (2) apply the modeling code to experimental fluid data obtained from weathering synthetic martian basalt. The modeling results provide useful comparisons between what can be expected to form in a closed chemical system upon evaporation and what is observed at the Meridiani Planum landing site. The stability of the resulting evaporite assemblages in contact with later fluids is also modeled, testing hypotheses related to Meridiani diagenesis.

2. Meridiani Planum: a unique geochemical system

Much of the data returned from the Meridiani landing site relates to the characterization of an impure evaporite unit, with analyses extending from "Eagle" crater (the initial landing site) approximately 750 m to "Endurance" crater and beyond [1]. Available data show that Meridiani outcrop contains four main components: (1) a siliciclastic component, possibly representative of basaltic material and/or other siliceous alteration phases, (2) hematite concentrated in nodules, (3) a phase or phases containing octahedrally coordinated Fe^{3+}, and (4) a sulfate-rich evaporitic component [1,13–15].

Evidence for the siliciclastic component comes from data collected by the alpha particle X-ray spectrometer (APXS). APXS data show that in addition to elevated sulfur (interpreted as the oxidized anion SO_4^{2-}), the outcrop generally displays elevated abundances of Si, Fe, Mg, Al and Ca [15]. Mössbauer analyses show that a minor portion of the outcrop is similar in Fe mineralogy to basaltic soils analyzed on the plains [13]. Further constraints on the chemical and mineralogical nature of this siliciclastic component are discussed by Clark et al. [16] and McLennan et al. [17].

In addition, Mössbauer spectroscopy indicates that hematite in the outcrop occurs in two forms: hematite within the grey, spherical nodules and hematite that is distributed within the outcrop (nodule-free). The Mössbauer spectrometer has also identified a phase or combination of phases contributing to an ambiguous spectral signature attributed to octahedrally coordinated Fe^{3+}. This feature is likely representative of poorly crystalline Fe-oxides, Fe-oxy-hydroxides, or Fe-sulfates. For example, some Mössbauer spectra acquired at Meridiani are identical to those produced by assemblages from Rio Tinto, Spain [5]. Such assemblages are comprised of schwertmannite, ferricopiapite, nanophase goethite, and other phases commonly associated with

jarosite (unless specified, "jarosite" used herein refers to all end-members) [5].

Except for Mössbauer identification of jarosite, the mineralogical nature of sulfates in the outcrop is under constrained. Non-jarosite sulfate may be bound to any combination of candidate cations, including Na^+, K^+, Ca^{2+}, Mg^{2+}, Fe^{2+}, Fe^{3+}, and Al^{3+}. Correlation between Mg, the most abundant available candidate ion, and SO_3 measured in the outcrop provide evidence that a Mg-bearing sulfate phase is an important component of the sulfate mineralogy [1]. Also, chemical un-mixing and detailed trend analysis of APXS data show that the outcrop likely contains a Ca-sulfate component [16,17].

Chlorides appear to be a minor component of the outcrop mineralogy, because Cl levels stay relatively constant with the exception of an increase a few meters into "Endurance" crater, where typical values of ~0.8–0.9 wt.% almost double [16]. The outcrop interiors (post-RAT) exhibit higher molar S : Cl ratios than the exteriors. The overall range is from about 5 to 30, consistently higher than measured at the Pathfinder and Gusev landing sites [15,18]. There are several minerals which contain both SO_4 and Cl ions in their structure and it is unclear in what form the Cl resides. Bromine to chlorine ratios vary considerably throughout the outcrop and are discussed in greater detail by Clark et al. [16].

In addition to the initial formation of outcrop evaporites, there is evidence that multiple diagenetic events affected outcrop mineralogy and geochemistry [1,17]. Diagenesis is important to the interpretation of evaporite geochemistry at Meridiani, because it suggests that the chemical and/or mineralogical nature of the outcrop as observed by *Opportunity* has been further modified after deposition as an evaporitic sandstone [17,19].

The emerging view of outcrop formation is one in which fluids initially derived from the weathering of basaltic material (likely driven by input of sulfuric acid) were subsequently evaporated, or frozen, leading to the precipitation of sulfate (and possibly minor chloride) minerals. The identification of jarosite suggests that the fluid from which the sulfate minerals precipitated was acidic. Sedimentological and stratigraphic evidence suggests that these chemical sediments were transported from an outside aqueous source (likely a dune-interdune-playa depositional setting) [19]. Syndepositional and/or subsequent diagenetic events formed conspicuous diagenetic features such as crystal-shaped molds, hematite-rich nodules, and areas where re-crystallization of cement is evident [17].

3. Thermodynamic modeling: background and approach

Calculations of mineral solubility based on thermodynamic data can provide important constraints on geochemical systems of interest. The solubility of a specific mineral requires the knowledge of its equilibrium constant (expressed here as $\log K$), which describes the activities of its components at equilibrium with a given fluid. Component activities, effectively thermodynamic concentrations, require accurate calculation of activity coefficients, which correct for non-ideal behavior of components in solution. The most common method used in calculating activity coefficients for concentrated or evaporating solutions (where non-ideality is substantial) is the specific ion interaction approach, which was improved upon largely by K.S. Pitzer and colleagues in the 1970s (see [9]). The Pitzer method accounts for the short-range electrostatic interaction between pairs of ions and triplets of ions, which becomes increasingly important as ionic strength increases (e.g., when water is removed by evaporation). This semi-empirical method has been employed with much success to model mineral solubilities in complex brines. For a given electrolyte, the interaction parameters required to model the activity of an aqueous component are: $\beta^{(0)}$, $\beta^{(1)}$, $\beta^{(2)}$, and C^{Φ}, which account for binary cation–anion interactions, θ for unlike cation–cation or anion–anion pairs, and Ψ for each cation–cation–anion and anion–anion–cation interaction [9]. These ion interaction parameters are usually evaluated from experimental measurements and sometimes from laboratory solubility data of minerals in electrolyte solutions of varying ionic strength [20,21].

In the calculations described here, we employ Pitzer's ion interaction approach, expanding the original thermodynamic dataset published by Harvie et al. [22] (referred to as HMW) to include interaction parameters for Fe^{2+} and Fe^{3+}. The HMW model is parameterized for the Na–K–Mg–Ca–H–Cl–SO_4–OH–HCO_3–CO_3–CO_2–H_2O system. The HMW model and the expansion used in this study are parameterized for 25 °C and as a consequence, all calculations discussed below are performed at that temperature. Ultimately, as available thermodynamic data improve, Fe geochemistry related to Mars must also consider temperature effects. The inclusion of both Fe^{2+} and Fe^{3+} in this model requires knowledge of interaction parameters with each component of the model. Our model does not include CO_2 or related aqueous species because experimental data with which to add this component to a system containing

Fe^{3+} are insufficient. Conclusive evidence for carbonates at the Meridiani Planum site is lacking and SO_4 appears to have been the primary anion and source of acidity (as H_2SO_4) in the system. In addition, carbonate precipitation (even under high pCO_2) is not expected to occur in this system until pH ~6–8, when siderite ($FeCO_3$) precipitates (e.g., [23]). Nevertheless, hypotheses of evaporite formation at Meridiani that include carbonate formation will need to be tested in the future.

Both ferrous and ferric iron must be included in this system because past redox conditions are generally unconstrained with respect to the Meridiani site. Despite identification of the ferric-iron bearing minerals jarosite and hematite, there remains some question as to what the redox conditions were throughout weathering, evaporation and diagenesis. The inclusion of both Fe^{2+} and Fe^{3+} in the model allows only redox disequilibrium with respect to the Fe(II)/Fe(III) couple to be evaluated. To simulate Fe redox disequilibrium, the Fe^{2+}/Fe_{Total} ratio of the input fluids can be changed and for the remainder of the discussion, we will express Fe redox disequilibrium in terms of this ratio. The Fe mineralogy at Meridiani Planum is clearly complex and the evaluation of redox conditions with respect to Fe in this model is an important and unique capability.

Table 1
Aqueous components and Fe-bearing minerals added to the thermodynamic database and other phases mentioned in the text

Phase/component	Formula	$\log K$	ΔG_f° (kJ mol^{-1})	Note
Fe^{2+} (aq)	–	–	−90.50	1
Fe^{3+} (aq)	–	–	−16.28	1
H_2O	–	–	−237.1826	2
SO_4^- (aq)	–	–	−744.46	3
K^+ (aq)	–	–	−282.46	3
Na^+ (aq)	–	–	−261.88	3
OH^- (aq)	–	–	−157.2	3
Bilinite	$Fe^{2+}Fe_2^{3+}(SO_4)_4 \cdot 22H_2O$	−15.9641	−8410	4
Copiapite	$Fe^{2+}Fe^{3+}4(SO_4)_6(OH)_2 \cdot 20H_2O$	−22.8912	−9971	4
Coquimbite	$Fe_2^{3+}(SO_4)_3 \cdot 9H_2O$	26.2707	−4250.6	4
$Fe(OH)_3$ (ppd)	$Fe^{3+}(OH)_3$ (ideal)	3.4562	−708.1	5
$FeSO_4$	$Fe^{2+}SO_4$	1.1650	−828.3	4
$Fe_2(SO_4)_3$	$Fe_2^{3+}(SO_4)_3$	2.0165	−2254.4	6
Ferricopiapite	$Fe_5^{3+}(SO_4)_6O(OH) \cdot 20H_2O$	−23.2801	−9899	4
Goethite	$Fe^{3+}O(OH)$	0.3671	−488.55	7
Hematite	$Fe_2^{3+}O_3$	−0.2266	−745.401	8
Jarosite-H_3O	$(H_3O)Fe_3^{3+}(SO_4)_2(OH)_6$	−6.0059	−3232.3	9
Jarosite-K	$KFe_3^{3+}(SO_4)_2(OH)_6$	−11.6511	−3309.8	9
Jarosite-Na	$NaFe_3^{3+}(SO_4)_2(OH)_6$	−5.9538	−3256.7	9
Kornelite	$Fe_2^{3+}(SO_4)_3 \cdot 7H_2O$	23.2110	−3793.7	4
Lawrencite	$Fe^{2+}Cl_2$	9.0945	−1264.29	7
Melanterite	$Fe^{2+}SO_4 \cdot 7H_2O$	−2.1937	−2507.75	4
Roemerite	$Fe^{2+}Fe_2^{3+}(SO_4)_4 \cdot 14H_2O$	−11.3146	−6486	4
Rozenite	$Fe^{2+}SO_4 \cdot 4H_2O$	−2.0181	−1795.2	4
Siderotil	$Fe^{2+}SO_4 \cdot 5H_2O$	−2.2840	−2033.9	4
Szomolnokite	$Fe^{2+}SO_4 \cdot H_2O$	−1.5885	−1081.2	10
Voltaite	$K_2Fe_5^{2+}Fe_4^{3+}(SO_4)_{12} \cdot 18H_2O$	−37.4515	−14,499	4
Anhydrite	$CaSO_4$	−4.3617	−1321.83	8
Epsomite	$MgSO_4 \cdot 7H_2O$	−1.8809	−2869.91	11
Gypsum	$CaSO_4 \cdot 2H_2O$	−4.5805	−1797.197	7

[1] ΔG_f° data from [30].
[2] ΔG_f° data from [31].
[3] ΔG_f° data from [32].
[4] $\log K$ calculated from ΔG_f° data (25 °C) reported by [33].
[5] $\log K$ calculated from averaged ΔG_f° data (25 °C) reported by [34].
[6] $\log K$ calculated from ΔG_f° data (25 °C) reported by [35].
[7] $\log K$ calculated from ΔG_f° data (25 °C) reported by [36].
[8] $\log K$ calculated from ΔG_f° data (25 °C) reported by [37].
[9] $\log K$ calculated from ΔG_f° data (25 °C) reported by [38].
[10] $\log K$ calculated from ΔG_f° data (25 °C) reported by [39].
[11] $\log K$ calculated from ΔG_f° data (25 °C) reported by [22].

Pitzer ion interaction parameters for Fe^{3+} are scarce and few experimental data required for their determination exist in the literature. Until a fully tested set of experimentally derived ion interaction parameters exist, alternative methods of modeling Fe must be used. Previous studies of Pitzer model expansion have used ion interaction parameters for analog ions, usually of similar size and charge. We adopt the same method, using a partial set of ion interaction parameters (for our system) recently published for Fe^{2+} and Fe^{3+} and obtaining the majority of remaining parameters from other analog data for trivalent ions such as Al^{3+}. While adequate for our purposes, the resulting dataset provides only an interim solution to the lack of available experimental data determined for Fe^{3+}.

The ion interaction parameters chosen for this study and their sources are listed in supplemental datasets accompanying this paper. To model Fe^{2+}, we have used binary and ternary ion interaction parameters relevant to our system from previous studies [11,24,25]. Expansion of the database to include Fe^{3+} incorporates parameters from Christov [25]. Various substitutions were made using reported parameters for Al^{3+} [26–28]. Others were made by substituting known Fe^{3+} interaction parameters for one ion with another ion of similar charge. Also, the first hydrolysis species for Fe^{3+}, $FeOH^{2+}$, was added to the database (using the association constant from the LLNL thermochemical database [29]). However, no interaction parameters for $FeOH^{2+}$ were added. The pH of the first hydrolysis reaction at 25 °C is approximately 2.2. Since the second hydrolysis reaction of Fe^{3+} is not included, the maximum pH at which the model has been tested and is considered to produce reasonably accurate results is a pH lower than the value at which a significant fraction of dissolved Fe^{3+} exists as $FeOH^{2+}$. We have determined this limit to be approximately pH 4.

As stated above, calculation of mineral solubility also requires the knowledge of equilibrium activity values, which are reflected in the equilibrium constant for a given mineral. Several Fe-bearing minerals were added to the thermodynamic database used in this model. The Fe-bearing minerals added to the database, their formulae, $\log K$ values, and sources of the data are listed in Table 1. Several equilibrium constants for Fe-sulfate minerals were calculated from Gibbs free energy of formation (ΔG_f°) values reported by Hemingway et al. [33]. In addition, ΔG_f° values for three end members of jarosite (K, Na, and H_3O) were added using data recommended by Drouet and Navrotsky [38]. Data for an ideal ferrihydrite composition (listed in Table 1) were added from Majzlan et al. [34]. Goethite and hematite were added by recalculating ΔG_f° values in the LLNL database [29,40] using our chosen ΔG_f° values for aqueous species used in all other calculations to maintain consistency.

All of the thermodynamic modeling presented in this paper was performed with the program React, which is part of the software package, *The Geochemist's Workbench* ® (GWB) [40]. React includes a thermodynamic database from the PHRQPITZ program [41], an extension of the HMW [22] database of ion interaction parameters and equilibrium constants. The ion interaction parameters and equilibrium constants in this database were modified as described above. React is a program which traces reaction paths in a given system by iteratively calculating its equilibrium state. More details on both the software and its thermodynamic principles can be found in [40,42].

4. Thermodynamic modeling: assessment of accuracy and limitations

Before applying the model to our input database of solutions, it is necessary to assess the accuracy of the calculated component activities in high ionic strength fluids. To do this, we have calculated the equilibrium state for complete water analyses from the Genna Luas mine site in Sardinia, Italy. Solution analyses were obtained from F. Frau, who collected and analyzed the samples and provided unpublished data accompanying a study done in 2000 [43]. These solutions were chosen because they include all of the components of our system of interest, including Fe^{2+} and Fe^{3+}, are acidic (pH between 0.4 and 3.5) and have high ionic strength (1–9 m). The calculated Fe^{2+} and Fe^{3+} activities for each water analysis are inserted into the Nernst equation to obtain a calculated Eh value at 25 °C:

$$Eh_{\text{calc}} = E_0 - RT\ln\left(\frac{a_{Fe^{2+}}}{a_{Fe^{3+}}}\right),$$

where E_0 is the standard electrode potential for the Fe couple at standard state (0.770 V), R is the ideal gas constant, and T is temperature in Kelvin [44]. There is substantial evidence that redox equilibrium is reached between dissolved Fe and the platinum electrode used to measure Eh in the field (an assumption in using the Nernst equation) [10,45]. Also, the high Fe concentrations of the natural waters used for comparison are ideal in that Eh measured at low concentrations of Fe (below about 10^{-5} m) sometimes reflects a mixed potential resulting from contribution from oxygen [10].

The agreement between measured Eh and calculated Eh values is depicted in Fig. 1. The calculated values

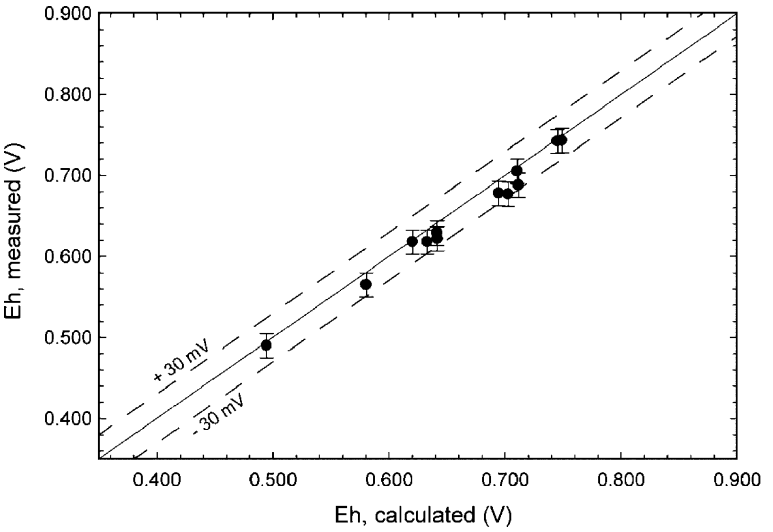

Fig. 1. Comparison of measured and calculated Eh values. Measured Eh values are from the Genna Luas Mine, Sardinia, Italy. The data include analyses reported in [43] and unpublished data from the same study. Measured pH ranges from 0.4 to 3.5 and calculated ionic strength ranges from 0.1 to 8.4 m.

agree with the measured values to within 30 mV. The typical error associated with Eh measurements in the field is approximately 15 mV. This relationship shows that the model can provide adequate estimates of Fe^{2+} and Fe^{3+} activities that are consistent with these field observations. A similar approach was used by Nordstrom and co-workers [45,46] to demonstrate the reliability of Fe activity calculation using speciation models at lower ionic strengths than those used here.

Finally, to assess the largest sources of error in our calculations, a sensitivity analysis on the modeling code was performed (supplemental dataset 2). In these calculations, error can come from three major sources: (1) analytical uncertainty in the input solution analyses, (2) uncertainties in the ion interaction parameter values used and (3) uncertainties in the $\log K$ values chosen or calculated for the model. The first source of error was evaluated in the sensitivity analysis by simply calculating the equilibrium state of one of the input solutions and not allowing precipitation to take place (therefore allowing saturation states of various minerals to be tabulated and compared). This result was then compared to duplicate calculations done one by one, but with one element of the input analysis decreased by 10%, to simulate a maximum in analytical uncertainty. The process was then repeated for the same solution, but concentrated by an order of magnitude to assess the same error at high ionic strength. The changes in saturation indices of relevant minerals were then tabulated and compared. Saturation index (SI) is a quantity which reflects the amount of departure from equilibrium of a fluid with respect to a given mineral phase. In Geochemist's Workbench, $SI = \log(Q/K)$, where Q is a ratio of component activities in the fluid and K is the ratio of component activities if the fluid is in equilibrium with respect to the mineral of interest. If $Q = K$, then the term in parentheses is 1 and $SI = 0$, indicating mineral saturation, or equilibrium between a fluid and mineral. If $Q < K$, the SI is negative and the fluid is under saturated with respect to the mineral of interest. Conversely, if $Q > K$, the SI is positive and the fluid is supersaturated with respect to the mineral of interest. During the sensitivity analysis, typical error in the saturation index of relevant minerals was on the order of 0.05 to 0.09 and was produced upon variation of Ca, Mg, Fe^{2+}, Na, and K. Varying Fe^{3+} produced the largest error, up to approximately 0.24 in the saturation index of the mineral ferricopiapite.

The second source of error was assessed by varying each ion interaction parameter added to the model (those including Fe) by 25%. The change produced in Fe^{2+} and Fe^{3+} activities, Eh, pH, and various mineral saturation indices upon parameter fluctuation was tabulated (supplemental dataset 2). The only significant errors were produced when the binary interaction parameters, $\beta^{(0)}$ and $\beta^{(1)}$, for Fe^{2+} and Fe^{3+} with SO_4^{2-} were changed. Large error upon variation of binary parameters was expected, as the Pitzer equations predict such an effect [9]. The most severe error accounted for a change in the saturation index of K-jarosite of 0.89. However, the published uncertainty for the Fe^{2+}–SO_4^{2-} and Fe^{3+}–SO_4^{2-} binary parameters is approximately 10% for $\beta^{(0)}$ and $\beta^{(1)}$ [11,25]. Overall, the ternary parameters result in negligible error within the 25% fluctuation.

The remaining source of error results from the treatment of equilibrium constant data. It is important to note that some data for Fe-sulfates obtained from Hemingway et al. [33] are only estimates based on the apparent absence of an excess enthalpy of mixing for the sulfate–H_2O system. Unfortunately, there are few experimental solubility data with which to compare these $\log K$ values. A thorough assessment of internal consistency for some of the new $\log K$ data added to this database is therefore prevented. However, some comparisons can be made. For example, the data for melanterite can be compared to those published by Reardon and Beckie [11]. Our calculated $\log K$ value (-2.194), using the reported ΔG_f° value from Hemingway et al. [33], agrees quite well with the value reported by Reardon and Beckie [11] at 25 °C (-2.205), which was based on solubility measurements. Similar deviations hold for Fe-bearing phases for which published thermodynamic data exist. Deviation between published ΔG_f° values is greatest for ferrihydrite because it normally occurs with variable composition and crystallinity.

Additionally, all of the minerals considered in these calculations are pure end-members; no solid solutions are used. Sulfate minerals often occur with some degree of solid substitution, which changes the Gibbs free energy of formation (ΔG_f°) for that particular mineral, and hence its solubility. Finally, because the forward modeling is based purely on thermodynamic constraints, it effectively ignores kinetic complications or barriers that are often encountered in natural systems [42,47,48]. Possible kinetic factors that apply to the system modeled here are discussed below. However, when considering evaporation paths, equilibrium modeling has produced exceptional results when compared to field observations in many prior studies (e.g., [22,49,50]) and therefore, the assumption of equilibrium when modeling evaporation is deemed acceptable. All of the above limitations and sources of error are important and should not be overlooked in further interpretation of the results presented here.

5. Applications to Meridiani Planum

5.1. Input data

In modeling evaporation processes at Meridiani Planum, we use the solution analysis dataset reported by Tosca et al. [51]. In their study, Tosca et al. [51] synthesized two crystalline basalts of martian composition and two pure basaltic glass compositions which were all reacted with a variety of acid mixtures (sulfuric to hydrochloric in a 4:1 molar ratio) for a total of 14 days each at 25 °C. The solution database obtained during that study provides a range of initial solution compositions that are taken to represent typical fluid chemistry resulting from weathering on Mars.

For the input data used in the present study, the S:Cl ratio of the fluids from Tosca et al. [51] was changed from 4:1, to 30:1, to maintain consistency with observed values of the Meridiani outcrop. The amount of SO_4 initially added to each experiment is reported in [51]. However, changing the S:Cl and Fe^{2+}/Fe_{Total} ratios in the fluid will change the pH. Charge balance of each input solution was therefore recalculated by varying Cl^- until a fluid composition was attained with the experimental pH and SO_4 values and a S:Cl ratio of approximately 30.

5.2. Physical representation of evaporation modeling

The GWB software offers two physical scenarios when modeling evaporation. The first scenario allows each mineral precipitated to back-react with the fluid of evolving composition. The fluid, therefore, maintains equilibrium with all of the minerals over each step of the calculation. Equilibrium requires that the number of mineral phases produced be constrained by the phase rule [42]. The other alternative is not to allow back-reaction of minerals with the fluid, which accounts for minerals that, for a variety of physical or chemical reasons, are unlikely to dissolve once they form. This scenario offers a more relevant physical representation of evaporation at Meridiani, because one can envision more than one mechanism by which minerals precipitated at the beginning of a sequence will be separated from the evaporating fluid. The sedimentology and stratigraphy of Meridiani outcrop provide several lines of evidence that the evaporite minerals were involved in both subaqueous and subaereal sedimentary environments, likely resulting in some degree of mineral fractionation during evaporation [17,19]. Examples of such processes include precipitation along the margins of a receding playa lake, or eolian scouring and transport from the sediment–water interface of an evaporating phreatic zone, creating a deflation surface. Grotzinger et al. [19] suggest that the Wellington contact observed at Burns Cliff, representing the boundary between dune and sand sheet facies, may be indicative of the latter process. Regardless, comparison of results from the two methods allows the identification of possible back reactions between mineral phases in this system.

5.3. Evaporites on Mars: comparison to Earth

Evaporite mineralogy is significantly controlled by fluid chemistry prior to evaporation. On Mars, where surface lithologies are largely basaltic, the chemistry of surface and sub-surface fluids is controlled by basaltic weathering. This unique geologic setting is fundamentally different than that of terrestrial evaporites (both marine and non-marine), which are dominated by ocean chemistry and by the chemistry of fluids controlled by weathering of the continental crust. Among many other factors, the chemical composition of weathering fluids can be controlled by variations in host-rock lithology, redox conditions, and the pH of weathering. The sensitivity of the modeling results to such important factors is discussed below. However, it is important first to distinguish the major differences that exist between typical surface fluids on Mars and Earth and how they translate into markedly different evaporite mineral assemblages.

Weathering martian basalt under acidic conditions will result in fluids that are enriched in Fe, Mg, SiO_2(aq), SO_4, and to a lesser degree, Ca (e.g., [51]). Carbonic acid (H_2CO_3) may have also been abundant, but the evidence is ambiguous, and for now we will focus more on the cation chemistry produced by rock weathering. In comparison to martian surface fluids, typical ocean water on Earth is dominated by Na, Cl, Mg, and SO_4 [52]. Average terrestrial river water is typically dominated by HCO_3, Ca, and SiO_2(aq) [52]. The chemical signature of seawater is influenced by input from weathering the continental crust (e.g., river influx) and factors such as mid-ocean ridge input [53]. The differences between terrestrial seawater and possible martian fluids are shown in Fig. 2. This comparison serves to illustrate major differences in anticipated martian evaporite mineralogy and typical marine evaporite mineralogy on Earth. For example, in contrast to terrestrial marine evaporites, elements such as Na and K are likely to play only a minor role in evaporite mineralogy on Mars.

Evaporites on Earth are typically dominated by halite, calcite, anhydrite and various K- and Na-containing chlorides and sulfates. In contrast, evaporite mineralogy on Mars is likely to be dominated by Mg-, Fe-, Ca-sulfates, and silica phases such as amorphous silica, if an acidic weathering regime prevailed. Figs. 3–8 show minerals precipitated and the major

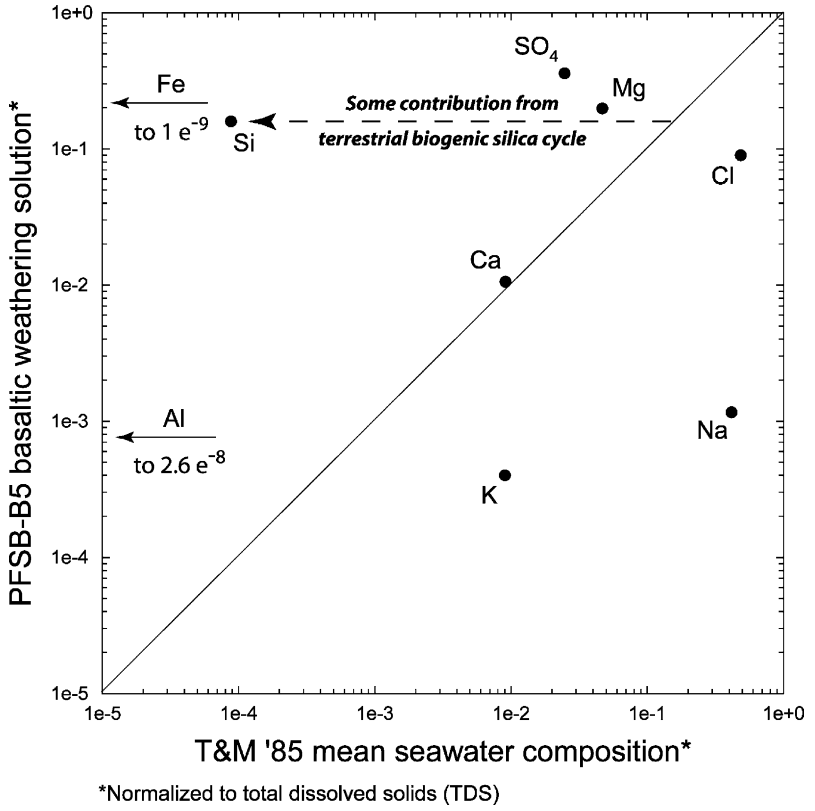

Fig. 2. Comparison of fluid chemistry obtained by weathering synthetic, olivine-bearing basalt (PFS) at pH 2, from [51] and mean terrestrial seawater composition from [52]. Both fluids are normalized to total dissolved solids.

element chemistry of the corresponding solution as basaltic weathering fluids are evaporated. In general, gypsum precipitates first, followed by more soluble Fe^{2+}-bearing sulfates and finally Mg-sulfates. Jarosite saturation and precipitation is almost always predicted at the outset because it is the most insoluble Fe^{3+}-bearing sulfate in the database.

Chemical and mineralogical data obtained from the martian surface show that several of the phases predicted to form in the calculations are indeed important to the evaporite mineralogy on Mars. New data from the OMEGA spectrometer aboard the Mars Express orbiter provide abundant evidence that at least Mg- and Ca-bearing sulfates (and possibly additional sulfate phases) are more abundant on the martian surface than previously thought [2,54–56]. In addition to growing spectroscopic evidence for Mg- [54,55], Fe- [57], and Ca-sulfates [54–56] at the martian surface, the globally homogeneous dust component on the upper most surface of Mars bears a strong Mg–SO_3 correlation, suggesting that Mg-sulfates are abundant enough to impart a global signature to the dust [58,59]. In addition, very high sulfate soils have now been discovered at Gusev Crater by the *Spirit* rover in both the Gusev plains regolith and in the Columbia Hills. In addition to SO_3, APXS data indicate that the soils also appear to

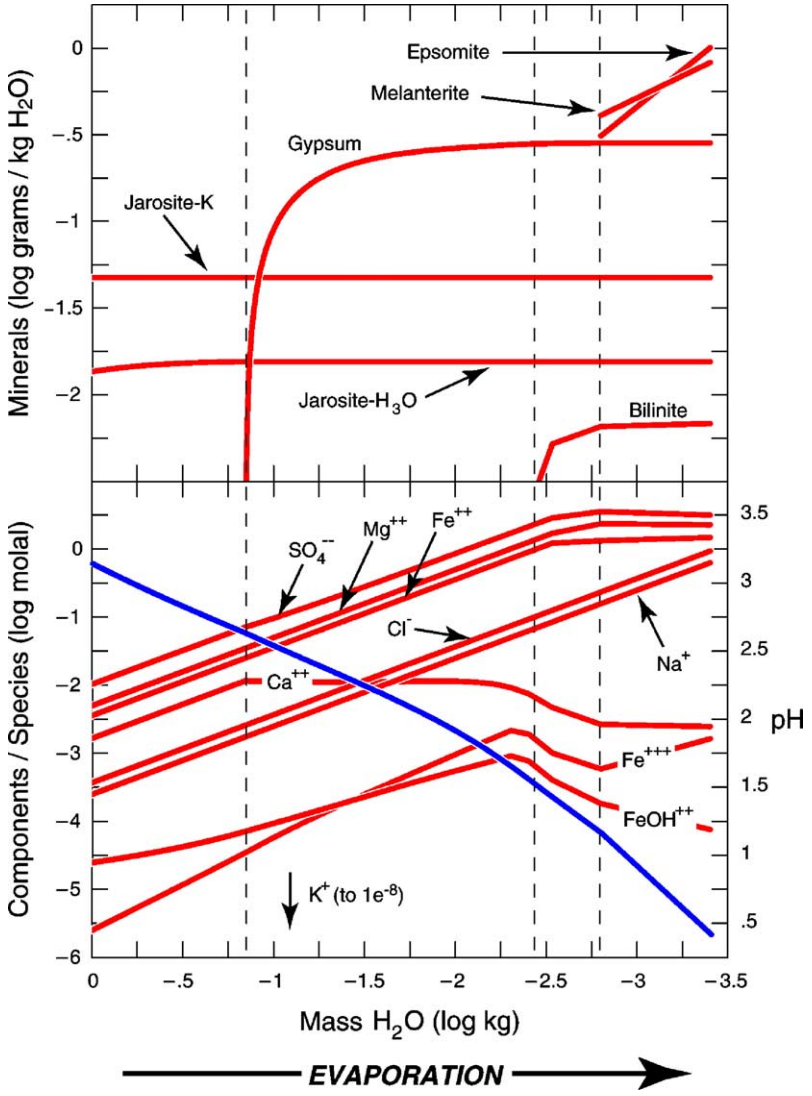

Fig. 3. Mineral precipitation and fluid chemistry predicted by modeling evaporation of a basaltic weathering-derived fluid. The fluid chemistry represents aqueous components rather than actual speciation because complex formation is treated within the Pitzer equations. The fluid was obtained by weathering synthetic olivine-bearing basalt. At the start of evaporation, pH ~3.2. $Fe^{2+}/Fe_{Total}=0.9$, no back reaction allowed. Suppressed mineral phases: goethite and hematite. The blue line indidicates pH on the right hand axis.

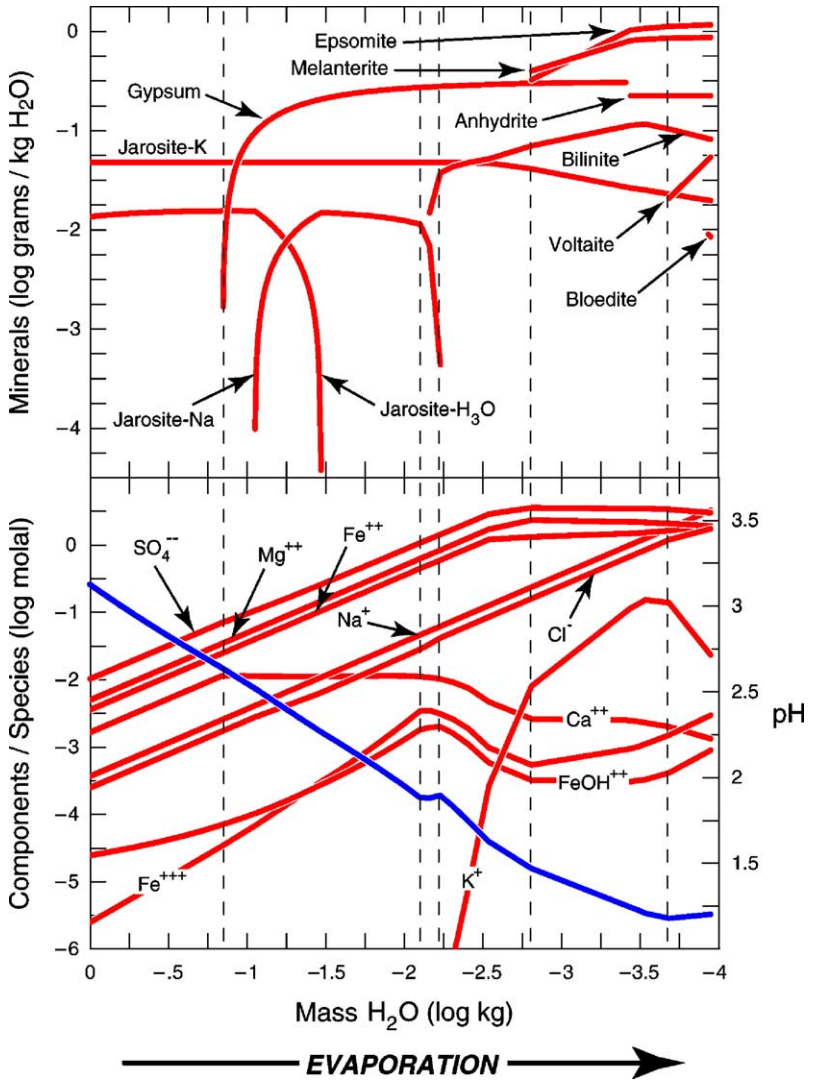

Fig. 4. Mineral precipitation and fluid chemistry predicted by modeling evaporation of a basaltic weathering-derived fluid. The fluid chemistry represents aqueous components rather than actual speciation because complex formation is treated within the Pitzer equations. The fluid was obtained by weathering synthetic olivine-bearing basalt. At the start of evaporation, pH ~3.2. $Fe^{2+}/Fe_{Total}=0.9$, back reaction allowed. Suppressed mineral phases: goethite and hematite. The blue line indidicates pH on the right hand axis.

be dominated by Mg in the Gusev plains regolith and Fe in the Columbia Hills [60–62].

The differences discussed above apply to a very large scale between Earth and Mars and underscore the uniqueness of evaporite assemblages produced on each. This view is, of course, simplistic and the amount of variation in martian fluid chemistry and evaporite mineralogy also needs to be assessed. The modeling calculations performed in this study attempt to capture some of the extent of variation that can be expected. The wide range in experimental fluid data in combination with the expanded thermodynamic model discussed above allows the sensitivity of evaporite mineralogy to factors such as lithology differences, degree of weathering (largely dictated by pH), Fe redox state, and mineral fractionation upon evaporation to be assessed.

5.4. Evaporites on Mars: controls by host lithology

The fluids used in this study were derived from basalts of two lithologies: olivine-bearing and non-olivine bearing basalts. Both basalts contained substantial clinopyroxene and plagioclase, with minor oxides and some interstitial glass (Fig. 9). The presence of olivine is clearly the most important factor in controlling the solution chemistry and this is reflected in the modeling

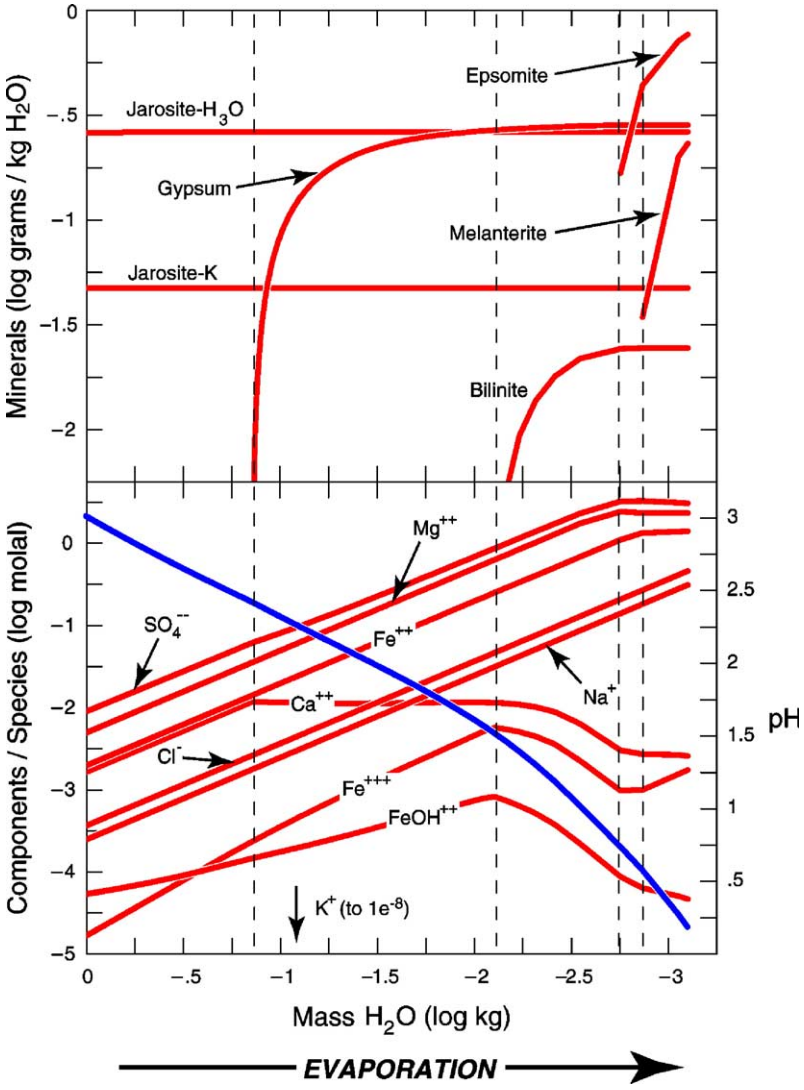

Fig. 5. Mineral precipitation and fluid chemistry predicted by modeling evaporation of a basaltic weathering-derived fluid. The fluid chemistry represents aqueous components rather than actual speciation because complex formation is treated within the Pitzer equations. The fluid was obtained by weathering synthetic olivine-bearing basalt. At the start of evaporation, pH ~3.1. $Fe^{2+}/Fe_{Total}=0.5$, no back reaction allowed. Suppressed mineral phases: goethite and hematite. The blue line indidicates pH on the right hand axis.

results. Upon evaporation of all solutions produced when weathering the PFS (olivine bearing) basalt, Mg-sulfates were formed, usually in significant quantities (e.g., Fig. 9). However, in none of the calculations did Mg-sulfates form upon the evaporation of fluids from the PFR basalt (containing no olivine). The Mg content in the PFR fluids remained low throughout the initial weathering experiments—a consequence of no olivine and low bulk Mg content. Also, the last iteration of the evaporation calculations using PFR fluids showed that Mg-sulfates were typically under saturated, with a saturation index of no greater than −2.0. This degree of under saturation cannot be explained by any of the error produced during the sensitivity analyses. In contrast to the PFR (non-olivine bearing) experiment, the PFS, or olivine-bearing basalt, shows that a significant fraction of Mg-sulfate is produced upon evaporation. Thus, olivine is clearly important in introducing enough Mg into the weathering solutions to produce significant amounts of Mg-sulfates upon evaporation.

5.5. Evaporites on Mars: control by pH of chemical weathering

Another significant control on the chemistry of weathering solutions and resulting evaporite mineral

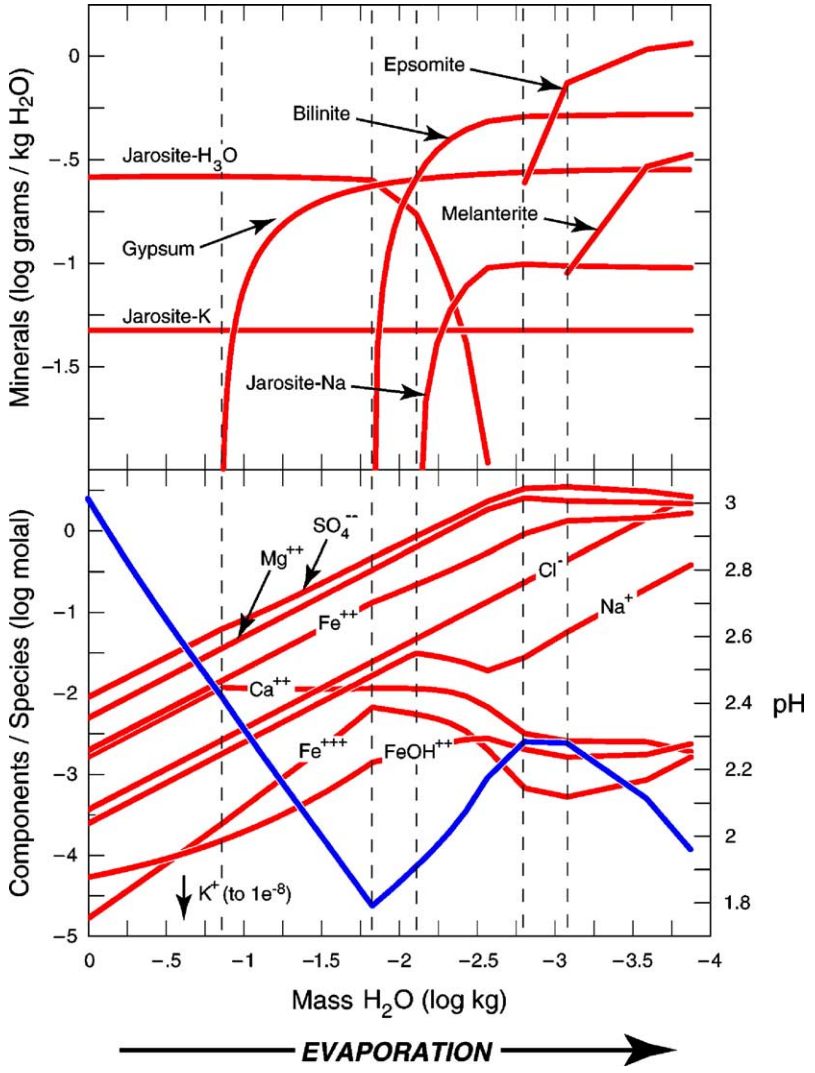

Fig. 6. Mineral precipitation and fluid chemistry predicted by modeling evaporation of a basaltic weathering-derived fluid. The fluid chemistry represents aqueous components rather than actual speciation because complex formation is treated within the Pitzer equations. The fluid was obtained by weathering synthetic olivine-bearing basalt. At the start of evaporation, pH ~3.1. $Fe^{2+}/Fe_{Total}=0.5$, back reaction allowed. Suppressed mineral phases: goethite and hematite. The blue line indidicates pH on the right hand axis.

assemblages is the pH of weathering. It is useful to divide weathering solutions into two classes based on acidity: high buffering capacity and low buffering capacity. As used here, high buffering capacity means that much more material can be dissolved before solution pH is buffered to the higher values typical of basaltic weathering on Earth (i.e., circum-neutral and higher). These solutions are usually more acidic and the chemistry is dominated largely by dissolution processes. Olivine would make the largest contribution to high buffering capacity solutions, releasing large amounts of Fe, Mg and silica into solution. Upon evaporation, such fluids would consequently produce large amounts of Fe and Mg sulfates. While Ca would be leached from pyroxenes and plagioclase, it would be in comparatively small amounts because of the dominant amounts of Fe, Mg and silica. Low buffering capacity solutions mean that the acid input is in competition with the buffering capacity of the basalt. Higher pH values can be expected and with weaker acids, the ionically bonded (or, "leachable") constituents of minerals, such as Ca in plagioclase and pyroxene, would dominate the solutions. Weathering experiments using low buffering capacity solutions have shown that the contribution of Mg from olivine to the fluid can be less than Ca (leached from pyroxene). The exact upper limit of the pH of these solutions depends on whether the fluid is in contact with the atmosphere, which could provide

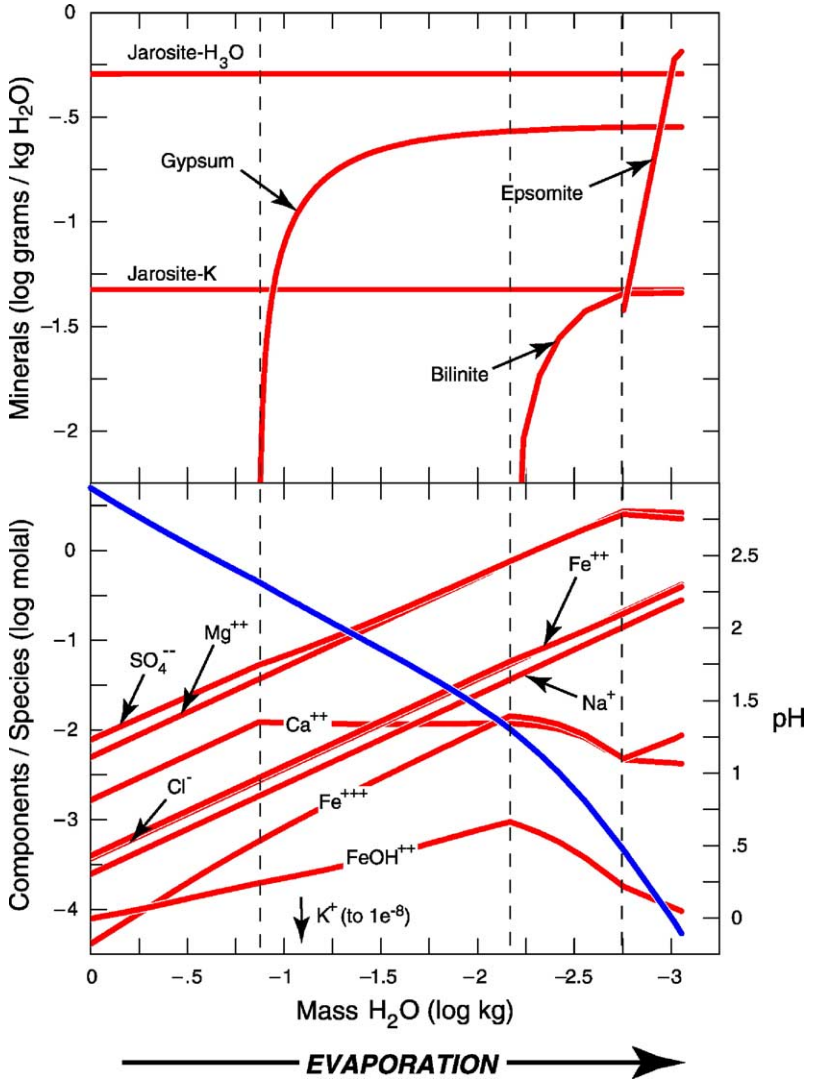

Fig. 7. Mineral precipitation and fluid chemistry predicted by modeling evaporation of a basaltic weathering-derived fluid. The fluid chemistry represents aqueous components rather than actual speciation because complex formation is treated within the Pitzer equations. The fluid was obtained by weathering synthetic olivine-bearing basalt. At the start of evaporation, pH ~3.1. $Fe^{2+}/Fe_{Total}=0.1$, no back reaction allowed. Suppressed mineral phases: goethite and hematite. The blue line indidicates pH on the right hand axis.

CO_2 or other volatile input, possibly lowering the pH. Evaporation of these solutions results in higher proportions of Ca-sulfates such as gypsum and anhydrite.

The results of the calculations performed in this study show distinct trends between evaporite mineralogy and pH of weathering. During the evaporation of fluids derived by weathering with progressively weaker acids (and having lower buffering capacity), the amount of gypsum systematically increases in all calculations. The amount of gypsum reflects the relative inputs from pyroxene and plagioclase, and a decreasing contribution from olivine. The weaker acid weathering solutions represent a "leaching" dominated regime. As a result, the evaporation calculations using the two weakest solutions for each basalt result almost entirely in gypsum and/or anhydrite. Ca is still an important element in the more acidic solutions, but is passively depleted because of high Fe and Mg abundances from olivine. Production of jarosite is unlikely in lower buffering capacity solutions, due to typically higher solution pH. Fig. 10 shows the trend produced for 4 weathering solutions, each increasing in initial weathering pH from pH 1.4 to 4.1. There is a clear decrease in epsomite and melanterite abundance and an increase in gypsum abundance, reflecting the transition to leaching-dominated weathering regimes.

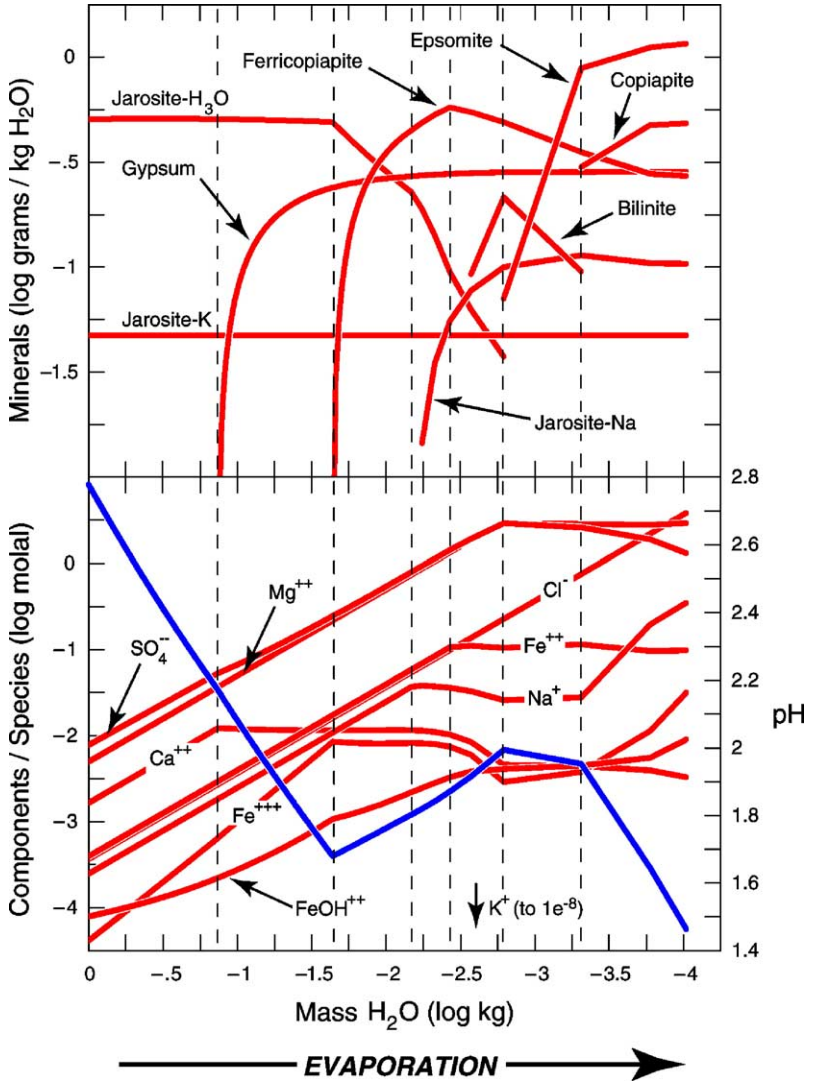

Fig. 8. Mineral precipitation and fluid chemistry predicted by modeling evaporation of a basaltic weathering-derived fluid. The fluid chemistry represents aqueous components rather than actual speciation because complex formation is treated within the Pitzer equations. The fluid was obtained by weathering synthetic olivine-bearing basalt. At the start of evaporation, pH ~2.8. $Fe^{2+}/Fe_{Total}=0.1$, back reaction allowed. Suppressed mineral phases: goethite and hematite. The blue line indicates pH on the right hand axis.

5.6. Evaporites on Mars: Fe chemistry and mineralogy

5.6.1. Fe(II) oxidation kinetics and redox disequilibrium

Iron is clearly an important component to consider in the interpretation of evaporite geochemistry on Mars, specifically at Meridiani Planum. Mössbauer analyses of outcrop material at Meridiani have revealed that approximately 90% of the total Fe resides in the Fe^{3+} state [13]. This observation implies that conditions were somewhat oxidizing in the initial altering fluid or during diagenesis, because basaltic weathering releases Fe^{2+} into solution and it must have been oxidized at some point during the evolution of Meridiani chemical sediments.

The kinetics of Fe(II) oxidation will control whether Fe is in equilibrium with $O_2(g)$ supplied to solution from the atmosphere. If the rate of Fe(II) oxidation is sufficiently slow, Fe and $O_2(g)$ will be in disequilibrium and both Fe^{2+} and Fe^{3+} will exist in solution. Although the oxygen content of the early martian atmosphere is poorly constrained, the few constraints on chemical conditions needed for the formation of Meridiani Planum evaporitic sediments suggest that Fe oxidation rates were indeed slow. For example, in addition to oxygen content, it has been well established that pH

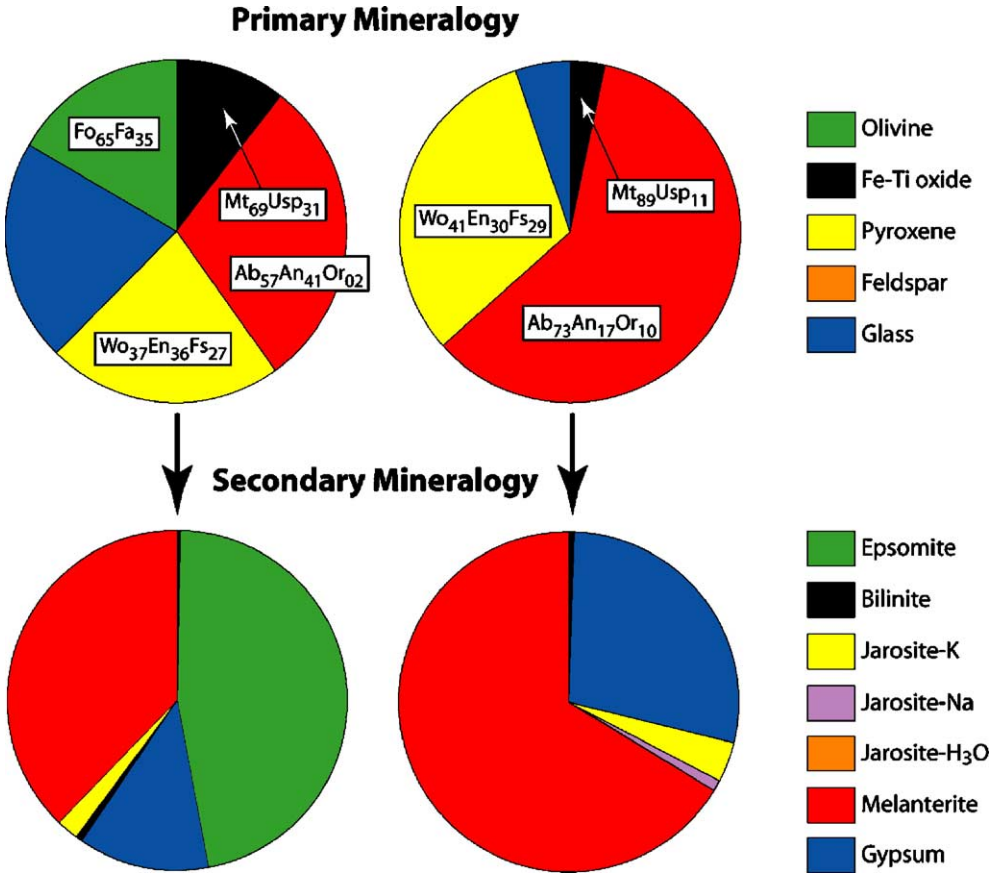

Fig. 9. The effect of basalt lithology on resulting evaporite assemblages (in wt.%). The olivine-bearing basalt results in Mg-sulfates, whereas the basalt with no olivine does not. Both evaporation models used fluids obtained by weathering basalts at approximately pH 3. $Fe^{2+}/Fe_{Total}=0.9$, no back reaction allowed. Suppressed mineral phases: goethite and hematite.

is a significant control on Fe(II) oxidation rates [63,64]. At pH levels greater than approximately 3.5, every unit increase in pH corresponds to a 100-fold increase in the Fe(II) oxidation rate [63]. The pH conditions needed for the formation of jarosite are generally lower than 3.5, suggesting that Fe(II) oxidation rates in Meridiani Planum fluids were slow and therefore independent of pH.

Although the rate of Fe(II) oxidation is difficult to quantify in this system, for our purposes it is valid to assume that over the time scales of acid sulfate weathering and surface evaporation, Fe was not in equilibrium with atmospheric oxygen and both Fe^{2+} and Fe^{3+} existed in solution. In fact, because Fe redox disequilibrium is so common in many aqueous environments on Earth, such an assumption is critical in adequately modeling geochemical systems that contain significant Fe, such as acid mine drainage environments [10,48]. The validity of assuming Fe redox disequilibrium in this system is also supported by Burns [65] who estimated that rates of Fe(II) oxidation on Mars for slightly acidic brines at current atmospheric conditions are approximately 4 orders of magnitude less than the same brines on Earth and 7 orders of magnitude less than oxidation rates in terrestrial river waters and oceans. Lastly, one important caveat to this discussion is that oxidation of Fe^{2+} (aq) has taken place only by molecular oxygen. Another process which may have contributed to oxidation of Fe^{2+} (aq) is UV photolysis, discussed in more detail by [65–67].

The inclusion of both Fe^{2+} and Fe^{3+} in the model discussed here allows the Fe^{2+}/Fe_{Total} ratio in the fluid prior to evaporation to be varied systematically, representing varying degrees of Fe redox disequilibrium. Since the actual mechanism and timing of Fe oxidation at Meridiani Planum is not constrained, we simply evaluate a variety of Fe^{2+}/Fe_{Total} ratios in solution before evaporation to assess possible formation pathways of Fe-bearing minerals.

5.6.2. Crystallinity effects on solubility

An important factor to consider in modeling the solubility of Fe^{3+}-bearing phases is the presence of

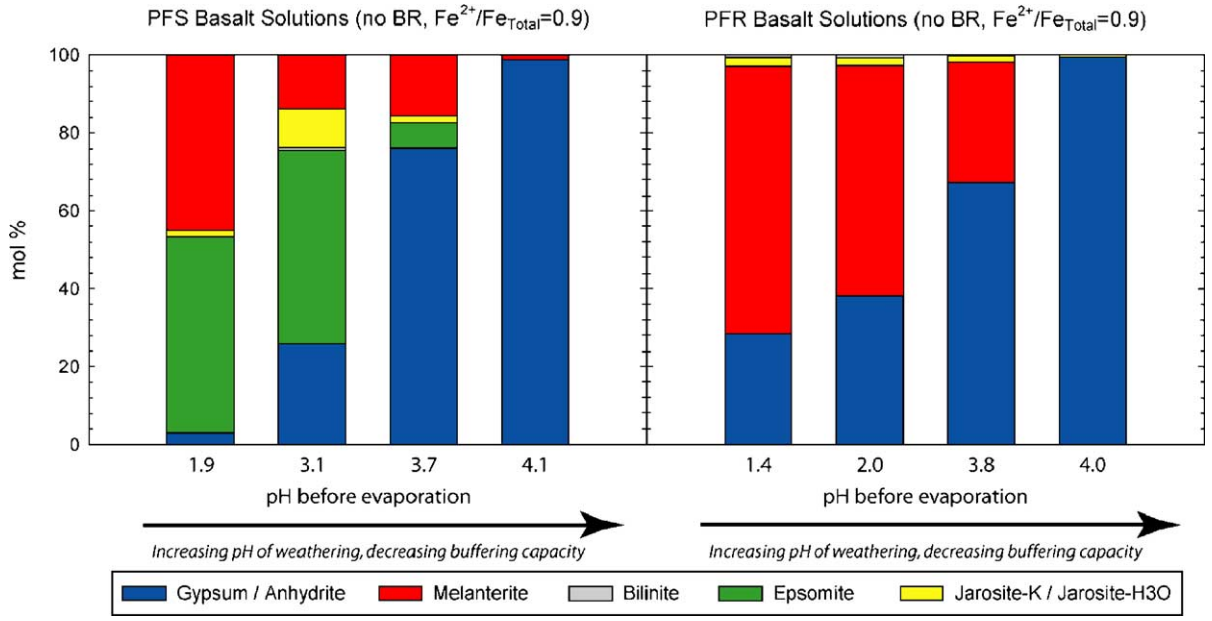

Fig. 10. The effect of initial weathering pH on resulting evaporite assemblages. As pH of weathering increases, weathering is dominated by leaching of soluble constituents and the assemblages contain a higher proportion of Ca-sulfates. At low pH, the PFS basalt is dominated by Fe^{2+}-sulfates and Mg-sulfates. All evaporation calculations use $Fe^{2+}/Fe_{Total}=0.9$, no back reaction allowed. Suppressed mineral phases: goethite and hematite.

poorly crystalline Fe-oxides, oxyhydroxides and hydroxysulfates. Such poorly crystalline phases are ubiquitous in acid mine drainage environments because the growth kinetics of goethite and hematite are slow at low temperature [68]. Consequently, the initial products of Fe oxidation and Fe(III) hydrolysis are poorly crystalline, fine-grained materials that are difficult to structurally characterize, and hence, difficult to measure for consistent thermochemical data. Most importantly, however, the particle size of such materials will have a direct effect on solubility (i.e., the $\log K$ value).

Particle size effects on solubility have been corroborated by much laboratory and field evidence and accordingly, have implications for some of the thermodynamic data discussed in this model as well as Fe-mineral stability relationships in the Meridiani outcrop (e.g., [69–71]). The stability boundaries predicted between Fe^{3+}-bearing phases (e.g., jarosite–goethite, and goethite–hematite) are somewhat uncertain given available thermodynamic data. The uncertainty arises because the crystallinity of jarosite, goethite and hematite can vary, causing phase boundaries to shift in pH. For example, in assessing schwertmannite and goethite stability, Bigham et al. [72] estimated the effect of sub-micron particle size on the $\log K$ of goethite and found phase boundary uncertainties of approximately 2 units in pH. Unfortunately, the thermodynamic data used in the present study cannot fully account for such effects, and therefore, pH boundaries with respect to these phases must be interpreted accordingly. Although jarosite is normally found in a well-crystalline form and of somewhat large grain size, it can also precipitate with submicron particle size and consequently suffer from grain size effects on stability relations.

In general, crystalline, well-ordered goethite is uncommon in acid sulfate waters. Instead, freshly precipitated goethite is almost always found with a particle size of less than 0.1 μm in most sediments [68]. The overall effect is that with respect to coarse grained hematite, fine grained goethite (microcrystalline or nanocrystalline) becomes unstable under a broader range of conditions common to low-temperature sedimentary environments on Earth [70]. Two additional factors controlling the transition from goethite to hematite are temperature and relative humidity (i.e., partial pressure of $H_2O(g)$). In general, coarse-grained goethite is stable relative to coarse-grained hematite in liquid water up to ~80 °C [70]. However, calculations by Langmuir [70] show that at 1 bar total pressure, fine-grained goethite (less than 0.1 μm particle size) is unstable relative to coarse-grained hematite at all relative humidities and temperatures below 100 °C. Therefore, the $\log K$ chosen for goethite in this study (Table 1) can be viewed as representative of well-crystalline, coarse-grained goethite only.

Interestingly, a component identified by the Mössbauer spectrometer in almost all outcrop spectra (the so-called Fe3D3 component) has been assigned to an octahedrally coordinated Fe^{3+}-bearing phase and could be representative of any combination of the phases discussed above, including: superparamagnetic hematite or goethite, lepidocrocite, akaganeite, schwertmannite, ferrihydrite and certain phyllosilicates [13]. Any of the Fe-oxide, oxyhydroxide or hydroxysulfate phases may have formed during acid sulfate weathering, evaporation, diagenesis, or any combination of such processes. Consequently, the Fe3D3 component could represent the typically observed kinetic pathway for Fe(III) precipitation common in Fe-rich acid sulfate environments on Earth.

5.6.3. Controls on Fe(III)–SO_4 solubility in acid sulfate systems

Several different mineral phases have been found to exert control on Fe(III) and SO_4 concentrations in acid sulfate waters, and the treatment of such a complication is an important step when modeling evaporation in systems containing these components. Fluid pH and SO_4 activity appear to be among the most important factors in determining the nature of initial Fe-bearing phases precipitated from Fe-rich acid sulfate waters. In acid–sulfate systems, jarosite usually precipitates from solutions with a pH of about 1–3. At slightly higher pH levels (about 2.5–6), most acid–sulfate waters initially precipitate schwertmannite (nominally $Fe^{3+}O(OH)_{3/4}(SO_4)_{1/8}$), a poorly crystalline Fe-hydroxysulfate [72]. Schwertmannite may convert to either goethite or jarosite, depending on the pH and Fe^{3+}, SO_4, and K or Na activities in solution [73,74]. At a broader range of pH, but generally higher than ~pH 3–4, ferrihydrite (nominally $Fe^{3+}(OH)_3$) forms, which can convert directly to hematite (if pH is between 5 and 9) or to goethite [34,75]. These poorly crystalline materials often occur as mixtures in nature and in general, when outside their respective stability fields, these phases readily convert to jarosite or goethite [73].

In this study, pH of the input solutions chosen for evaporation ranges from about 1 to 4. Much laboratory and field evidence suggest that the phases largely controlling the initial Fe(III) and SO_4 concentrations in Fe-rich acid–sulfate waters of this pH range are jarosite (at the lower end of the range) and schwertmannite (at the higher end of the range) [68,72]. Schwertmannite may have played a role in controlling Fe(III) and SO_4 concentrations at least upon initial formation of acid sulfate weathering solutions where Fe(III) concentrations increased from Fe^{2+}(aq) oxidation. However, schwertmannite is not included in the present form of the modeling code because of large variations in composition and consequently, solubility estimates. Instead, we allow only jarosite to control initial Fe(III) and SO_4 concentrations and, owing to its ubiquitous presence in the Meridiani outcrop, suggest that jarosite eventually became a dominant phase in controlling the concentrations of these two components.

Given the above controls on Fe(III) concentrations, goethite formation upon all evaporation simulations is suppressed. Under the pH range of about 1–4 in acid sulfate waters on Earth, goethite is typically found in trace to minor amounts and control of Fe(III) concentrations by goethite is minor compared to jarosite and schwertmannite [68,72]. In addition, as discussed above, crystalline goethite (for which the calculated $\log K$ is the most representative) is uncommon in acid sulfate waters. Therefore, we assume that the same relationships hold in Fe-rich acid sulfate waters that have evolved from a basaltic substrate. The resulting configuration of the modeling code at the beginning of evaporation calculations represents a metastable equilibrium state; while the initial fluids are supersaturated with respect to goethite, the reaction to precipitate this mineral is unlikely to reach equilibrium over our time scale of interest [42]. Such a configuration of the modeling code however, does not imply that goethite cannot form during weathering or evaporation, it simply provides the most relevant scenario where Fe(III) and SO_4 concentrations are controlled by Fe-sulfates and not by Fe-oxyhydroxides during the evaporation process.

In diagenesis calculations described below, goethite is allowed to form because sediment–water interaction upon fluid recharge and diagenesis is likely a much closer approach to equilibrium than surface precipitation during evaporation. Hematite is suppressed in all calculations because under the low-temperature conditions considered here, goethite is likely the stable phase in contact with aqueous solutions in this system [70]. If hematite formed under low-temperature conditions, it likely formed from a precursor such as goethite.

5.6.4. Fe redox disequilibrium calculations

In one sub-set of calculations performed in this study, the Fe^{2+}/Fe_{Total} molar ratio in the fluids was varied from 0 to 1, in increments of 0.1 (equating to an Eh specific to the Fe couple of 0.760 V at 0.1 and 0.653 V at 0.9). The pH of each calculation was set to 3.0 and SO_4^{2-} was used to balance the difference in charge produced by changing the Fe^{2+}/Fe_{Total} molar

ratio. The overall change in SO_4^{2-} concentration is minor between the end-member calculations, ranging from 0.01104 to 0.01074 m. This change in SO_4^{2-} only changes the saturation index of gypsum from −0.9941 to −1.0007 between calculations and is an insignificant factor in changing the saturation index of Fe-sulfate minerals as well. Fig. 11A shows the percentages (in wt.%) of minerals produced upon evaporation of a solution derived from weathering an olivine-bearing basalt. It is clear that increasing the amount of Fe^{2+} in the solution results in a larger proportion of Fe^{2+}-sulfates, such as melanterite. As Fe^{3+} is increased, mixed-valence Fe sulfates increase in small amounts and the amount of jarosite (K and H_3O only) increases substantially to a maximum of 36 wt.%. Natrojarosite precipitates in very few calculations, which is likely a combination of limiting Na content and high acidity, favoring the K and H_3O end members. In general, for natrojarosite to precipitate, Na activity must be quite high relative to K activity. For example, Alpers et al. [76] found that log aqueous activity ratios for $(Na^+)/(K^+)$ must at least be higher than about 2.9 to 3.8 for natrojarosite to precipitate. It is interesting to note that in terms of actual moles precipitated, K-jarosite remains at the same value for almost every calculation increment, while H_3O-jarosite steadily increases (Fig. 11B). This trend is a result of a limiting K concentration, whereby the amount of K-jarosite precipitated per kilogram of solution is dependent on the amount of K present. As K generally remains low in the solutions encountered when weathering martian basalt, the amount of K-jarosite is also limited to small amounts. This result is consistent with Mössbauer measurements on the jarosite at Meridiani Planum, which suggest that the mineral must be an impure phase with respect to the K, Na and H_3O end-members. Furthermore, others [1,16,17] have noted that the jarosite present at Meridiani must be of limited K content by mass balance calculations in the outcrop.

The prediction of jarosite saturation at the outset of most calculations suggests that several basaltic weathering fluids relevant to Mars may be saturated with respect to jarosite. However, in many aqueous environments on Earth, waters are often saturated or supersaturated with respect to jarosite, yet jarosite is not frequently detected [73,77]. This is caused by kinetic limitations involved in jarosite precipitation, and comparable factors may be operable on the martian surface as well. As a result, jarosite formation at Meridiani Planum may occur either by initial chemical weathering of basalt (i.e., sediment–water interaction) or by evaporative concentration, which are both jarosite precipitation mechanisms that are observed to occur on Earth (e.g., [78,79]).

5.7. Evaporites on Mars: mineral fractionation and back-reaction

As discussed above, the GWB software offers the option to allow minerals to back-react, or to be removed from the fluid upon precipitation. Back reac-

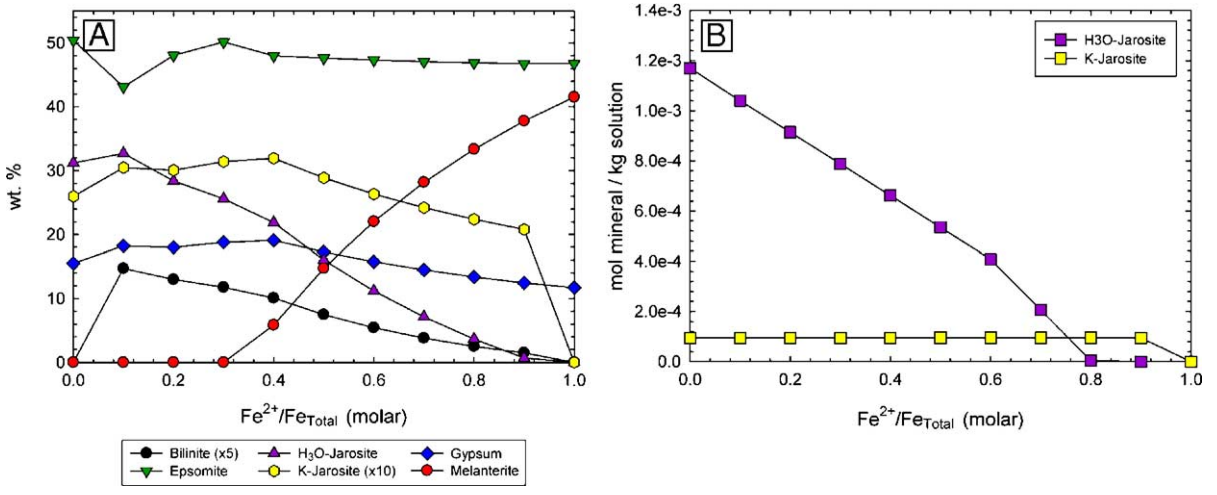

Fig. 11. The effect of varying Fe^{2+}/Fe_{Total} molar ratio in solution prior to evaporation (no back reaction). (A) As the Fe^{2+}/Fe_{Total} ratio is increased, the proportion of Fe^{2+}-bearing sulfates increases, while Fe^{3+}-bearing sulfates decrease. Bilinite (a mixed-valence Fe sulfate) and the jarosite end-members decrease as the ratio is increased. (B) K-jarosite abundance is limited by K content in solution and is produced in the same absolute concentration in each calculation. Excess Fe^{3+} is precipitated as H_3O-jarosite. All evaporation calculations suppress goethite and hematite. Prior to evaporation, pH was held constant at ~3.0.

tion is an important control to discuss, because it can be responsible for the presence or absence of particular minerals. With the exception of the gypsum–anhydrite dehydration reaction, all other back reactions occur between Fe-bearing mineral phases. Figs. 3, 5, and 7 show mineral precipitation and corresponding fluid chemistry during evaporation of a fluid derived from weathering olivine bearing basalt with back reactions allowed to take place over the course of the calculations. A common back reaction to appear upon evaporation is a result of end-member treatment of the jarosite phases; H_3O-jarosite dissolves and forms the Na-jarosite end member, which is a result of high Na activity by evaporative concentration and low K activity caused by prior K-jarosite precipitation. In general, jarosite precipitated at the beginning of evaporation calculations tends to dissolve and re-precipitate as mixed-valence Fe-bearing sulfate phases at intermediate to late stages of evaporation (i.e., low pH and high Fe and SO_4 activities). Fig. 12 illustrates the effect of different Fe^{2+}/Fe_{Total} ratios in solution on resulting mineral assemblages when back-reaction is allowed during evaporation. At high levels of Fe^{3+} in solution, large quantities of jarosite back-react to form ferricopiapite, an Fe^{3+}-bearing sulfate. As Fe^{3+} levels decrease, ferricopiapite disappears from the mineral assemblage and is replaced by mixtures of bilinite and copiapite, both mixed-valence Fe sulfate minerals. As Fe^{3+} is decreased further and Fe^{2+}begins to dominate the initial solutions, bilinite and copiapite become essentially exclusive of each other and the overall quantity of these phases decreases steadily until none are present at a Fe^{2+}/Fe_{Total} ratio of 1.0.

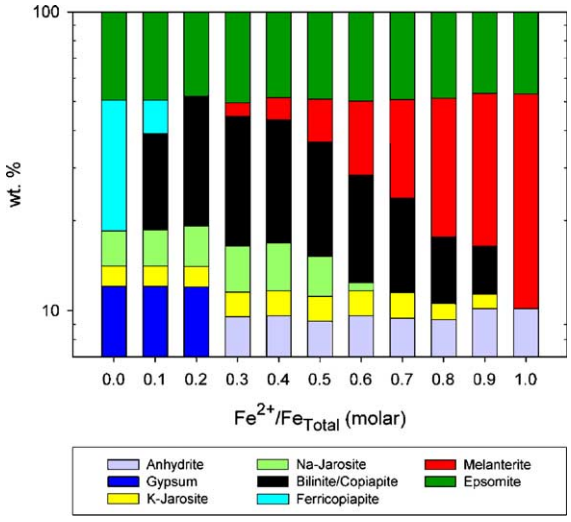

Fig. 12. The effect of varying Fe^{2+}/Fe_{Total} molar ratio in solution prior to evaporation (back reaction). As the Fe^{2+}/Fe_{Total} ratio is increased, the proportion of Fe^{2+}-bearing sulfates increases. Na-jarosite is produced at low ratios because of high Na/K activity ratios in the evaporating solution. At low Fe^{2+}/Fe_{Total} ratios, ferricopiapite dominates the mineral assemblage. As the ratio is increased ferricopiapite is no longer formed and is replaced by mixed-valence Fe-sulfates bilinite and copiapite. The overall mass of these materials decreases systematically with increasing proportions of ferrous Fe. All evaporation calculations suppress goethite and hematite. Prior to evaporation, pH was held constant at ~3.0.

A complicated set of phase relationships emerges when back-reaction at varying levels of Fe redox disequilibrium is considered. However, the general trend from dominantly ferrous sulfates to mixed-valence Fe sulfates and eventually to ferric sulfates as Fe^{3+} increases mimics trends found in the laboratory from evaporation experiments using waters derived from pyrite oxidation [80–82]. In addition to their application to evaporative settings, these phase relationships shed light on diagenetic reactions and the ultimate fate of such phases upon burial, dehydration, and/or oxidation, which is discussed in more detail below.

5.8. Evaporites on Mars: sediment diagenesis

Data collected from outcrop at Meridiani Planum show multiple lines of evidence for one or more diagenetic events after the initial formation of evaporite minerals [1,17]. The calculations discussed above represent mineral formation upon the evaporation of basaltic weathering fluids. The stability of these evaporite minerals in contact with later fluids is of interest for the interpretation of chemical diagenesis at Meridiani.

To model diagenetic reactions, we have taken a simple approach. The sedimentology and stratigraphy of the Burns Cliff section of outcrop analyzed at "Endurance" crater suggest that diagenesis was possibly mediated by a fluctuating groundwater table [19]. Accordingly, the diagenesis calculations shown here simulate fluid recharge into previously deposited evaporite sediments. The recharge process is modeled by first separating a mineral assemblage produced from evaporation modeling. The mineral assemblage was then reacted with an infiltrating fluid, at varying fluid-to-rock mass ratios. Varying the fluid-to-rock ratio controls the amount of solid in contact with an infiltrating fluid phase and by using molar volumes of minerals, can be expressed as total porosity. Porosity, as used here, is simply the volume fraction of fluid in the entire system and is an input parameter to the

diagenesis calculations. This type of calculation is often referred to as a "titration model", because the model literally "titrates" a given amount of mineral mixture into a volume of fluid, maintaining equilibrium during each step [42]. Detailed analysis of concretion sphericity shows that the average major axis of hematitic concretions in the outcrop is only slightly elongated (by ±6%), suggesting extremely slow fluid transport during the diagenetic event that initiated concretion formation [19]. Therefore, the configuration of the diagenesis simulations (fluid–mineral equilibrium in a closed system with no fluid transport) is an adequate physical representation of sediment–water interaction at Meridiani Planum. The model results are taken to be representative of how the initial evaporite portion of the rock will react with a pore fluid (Fig. 13). This modeling approach has been used in previous studies investigating sediment diagenesis (e.g., [42,83]).

Three sample mineral assemblages chosen to represent the evaporite portion of the outcrop before diagenesis are listed in Table 2. The evaporite assemblages were formed by simulating the evaporation of a fluid where Fe was in the dominantly ferric state (assemblage A), a mixture between ferrous and ferric (assemblage B), and in the dominantly ferrous state (assemblage C). The fluids, which may have been responsible for initiating later diagenetic reactions, are unconstrained and we have chosen to use only pure water to begin with. Water-to-rock mass ratios were varied in the calculations producing a range of 0.99 to 0.30 in porosity.

Fig. 14 depicts the resulting mineral assemblages, in mole percent, after diagenesis (using assemblages A, B, and C in Table 2). At high fluid-to-rock mass ratios (i.e., high porosity), most of the evaporite mineral assemblage dissolves into the infiltrating fluid. However, when the fluid-to-rock ratio is decreased, saturation is progressively reached with respect to each evaporite phase (from least soluble to most soluble). The diagenetic fluid therefore reaches a limiting saturation and ionic strength at a relatively low porosity value. A finite amount of each phase is lost to the fluid before saturation is reached and no additional mass is lost. At lower water-to-rock mass ratios (and lower porosity), a greater proportion of the initial evaporite assemblage is left intact. During fluid infiltration into sediment layers dominated by evaporite minerals, saturation with respect to soluble phases will likely be reached and these materials will be preserved. Alternatively, this simple concept can be expressed in terms of "pore fluid flushing events". Because a finite amount of material is dissolved during one diagenesis event, there will be a limit on how many events may take place before certain phases are dissolved. This assumes, however, that the dissolved components are transported away and "fresh" fluid is continuously re-introduced to prevent saturation or re-precipitation. Using a porosity of 0.30 (the highest value for which Mg-sulfates still reach saturation and are preserved in these calculations) and initially pure water, all of the epsomite and melanterite dis-

Table 2
Evaporite mineral assemblages used in diagenesis calculations (mole percent)

Mineral	Assemblage A	Assemblage B	Assemblage C
Epsomite	54.32	48.13	46.96
Gypsum	29.11	21.19	17.91
H_3O-jarosite	14.20	3.73	0.35
K-jarosite	1.67	1.22	1.03
Melanterite	–	25.52	33.67
Bilinite	0.66	0.20	0.08
Anhydrite	0.03	0.01	–
Initial Fe^{2+}/Fe_{Total}	0.30	0.70	0.90

Calculations performed with PFS basalt solution, pH ~3, no back reaction. Suppressed phases: hematite, goethite.

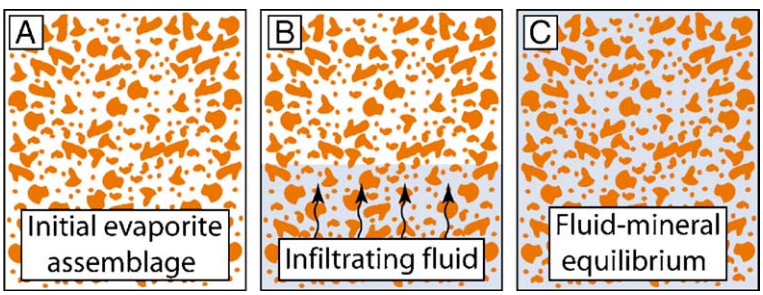

Fig. 13. Physical representation of diagenesis calculations. An initial evaporite mineral assemblage (A), is reacted with a volume of water (B) at a given rock-to-water mass ratio (or porosity). The calculations represent the attainment of equilibrium (C) between mineral phases and infiltrating pore fluid.

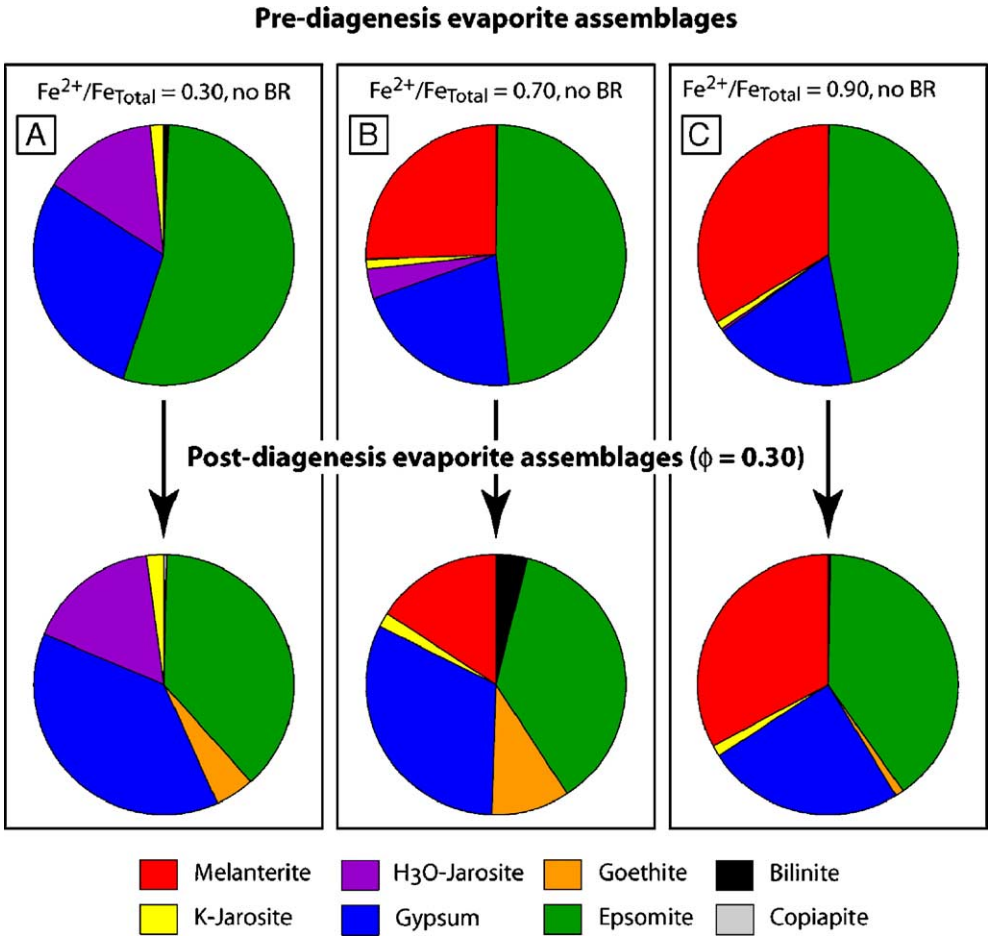

Fig. 14. Resulting mineral assemblages after diagenesis calculations (in mole percent). (A) Using evaporite assemblage A from Table 2, equilibrium between H_3O-jarosite and goethite is reached upon diagenesis, resulting in coexisting H_3O-jarosite and goethite in the post-diagenetic mineral assemblage. (B) Using evaporite assemblage B, goethite precipitation takes place, as well as the precipitation of mixed-valence Fe-sulfates, exhausting H_3O-jarosite completely. (C) Using evaporite essamblage C, goethite precipitation takes place with mixed-valence Fe-sulfates but is in comparatively small amounts. There is little overall change before and after diagenesis, with soluble components being preserved. The proportion of gypsum increases in all calculations as a result of lower solubility and less mass lost to the infiltrating solution. All calculations performed at 30% porosity.

solve after the second and third fluid flushing events, respectively. Because of its relative insolubility, gypsum is not completely dissolved until after hundreds of subsequent flushing events.

The effect of diagenesis on non-Fe bearing evaporite phases is relatively straightforward in that porosity controls the preservation of such soluble components. The composition of the infiltrating solution will have a similar effect. For example, an infiltrating brine would allow less mass to be dissolved if it were already close to saturation with respect to a certain mineral in the assemblage. It is important to note that primary sedimentary fabrics and textures of Meridiani outcrop show little disruption which may in fact indicate that the diagenetic fluid phase was highly concentrated in several major elements and relatively minor dissolution took place [17,19].

Fe-bearing evaporite phases, however, exhibit more complicated phase relationships upon diagenesis. In the diagenesis calculations described here, goethite is allowed to form because in this system, pore water interaction with reactive evaporite sediments is likely a closer approach to equilibrium than precipitation from surface evaporation combined with sedimentary transport, where we have assumed metastable equilibrium.

Upon equilibration of pre-diagenetic mineral assemblages with initially pure water, H_3O-jarosite dissolves, releasing Fe^{3+} into solution. In this system,

it is the fate of Fe^{3+} released by H_3O-jarosite (or other Fe^{3+}-bearing phases) that will determine possible changes in mineralogy upon diagenesis. Given the available thermodynamic data assembled for this study, Fe^{3+} released into solution may either reach saturation with respect to H_3O-jarosite, initially changing the character of mineral assemblages in a relatively minor way, or be precipitated into new diagenetic phases. If goethite is allowed to form, the continuous removal of Fe^{3+} from solution drives the transformation reaction until (1) saturation is reached with respect to H_3O-jarosite and equilibrium is reached between H_3O-jarosite and goethite, (2) H_3O-jarosite is exhausted resulting in complete transformation to goethite, or (3) a new diagenetic phase precipitates—a result of the chemistry of the diagenetic fluid being affected by the presence of other Fe- or SO_4-bearing minerals. The different end products depend on the mineralogical nature of the pre-diagenesis assemblage, most importantly in what proportion Fe is partitioned between ferrous and ferric phases. If goethite is not allowed to form over the course of the calculations, H_3O-jarosite simply reaches saturation and the resulting diagenetic mineral assemblage differs only slightly from the pre-diagenetic assemblage. However, in such a simulation, the diagenetic fluid, while in equilibrium with the mineral assemblage is highly supersaturated with respect to goethite and precipitation is still thermodynamically favored.

Fig. 14 shows the results of three diagenesis calculations using evaporitic mineral assemblages (listed in Table 2) where the Fe is partitioned mainly into ferric bearing materials (Fig. 14A), a mixture of ferric and ferrous bearing materials (Fig. 14B) and ferrous materials (Fig. 14C). The product of the first calculation is one where H_3O-jarosite equilibrium with respect to goethite was reached. In the second calculation, the pre-diagenetic assemblage contained melanterite, the dissolution of which resulted in a high amount of Fe^{2+} and SO_4^{2-} in solution, because melanterite is highly soluble. The calculation illustrates that releasing additional Fe^{3+} into a solution with high Fe^{2+} and SO_4^{2-} activities causes precipitation of mixed-valence Fe-sulfates (e.g., bilinite and/or copiapite) in combination with some goethite precipitation. The H_3O-jarosite is exhausted during such a process, because precipitation of both goethite and new mixed-valence phases maintains undersaturation with H_3O-jarosite until it is consumed. The final calculation shown in Fig. 14 is one in which the evaporitic mineral assemblage contained a significant amount of melanterite and comparatively little H_3O-jarosite. Saturation was reached with respect to melanterite, resulting mainly in preservation of all soluble components with little overall difference before diagenesis.

In each calculation shown in Fig. 14, H_3O-jarosite is the principal source for releasing Fe^{3+} into solution. Consequently, upon initial perturbation of evaporite mineral assemblages with water, goethite precipitation is thermodynamically favored. It is important to note that H_3O-jarosite and goethite are stable equilibrium phases and the transformation from H_3O-jarosite to goethite requires an aqueous phase low in Fe^{3+}, SO_4^{2-} and a pH of generally higher than 2–2.5. Furthermore, if equilibrium is established between goethite and H_3O-jarosite, the relative proportions of the two phases are dependent on factors such as the porosity and the amount of H_3O-jarosite and other Fe and SO_4 bearing phases initially present before diagenesis. The equilibrium reaction can be expressed for the H_3O end-member jarosite composition by:

$$(H_3O)Fe_3(SO_4)_2(OH)_6(H_3O\text{-Jarosite}) \Leftrightarrow 2SO_4^{2-} + 3FeOOH(\text{Goethite}) + H_2O + 4H^+.$$

Equilibrium relationships between jarosite and goethite are supported by countless field observations at acid mine sites on Earth, including Rio Tinto, Spain [5] and many others [e.g., 68,80]. The transformation of jarosite to goethite then, is a highly likely and thermodynamically favored reaction to control Fe(III) concentrations and Fe^{3+} mineralogy in diagenetic fluids. In the calculations described above, even though the initial fluid used is initially pure water, the pH of the infiltrating solution is quickly lowered to a value of approximately 2.0. This rapid decline in pH is controlled mainly by the equation listed above (an acid-generating reaction), and by the Fe^{3+} hydrolysis reaction. The dissolution of simple sulfate salts plays an indirect and minor role in affecting pH by changing sulfate–bisulfate speciation in the diagenetic fluid [84]. The overall chemistry of the diagenetic fluid, even when initially pure, is rapidly driven to an acidic, Mg, Fe and SO_4 dominated solution over the course of diagenesis calculations.

It is clear that the chemistry of diagenetic fluids will largely be determined by the reactivity of evaporitic sediments. Because the results described above suggest that diagenetic fluids are likely to have been acidic and Fe and sulfate rich, crystallization of poor-

ly crystalline goethite, which is commonly found under such conditions, may have occurred. One hypothesis, then, is that hematite concretions may have formed by the coagulation of poorly crystalline goethite. Conversion from poorly crystalline goethite to coarse-grained hematite is thermodynamically favored at all temperatures and relative humidities below 100 °C, [70] resulting in local equilibrium (i.e., within the concretions) which may have been established in response to evolving atmospheric conditions over time.

A final and important consideration for diagenesis is the fate of Fe^{2+}-containing sulfates upon prolonged exposure to an oxidant such as O_2(aq). The diagenesis calculations described here do not take into account changing redox conditions during the course of diagenesis (i.e., Fe^{2+}/Fe_{Total} in solution is determined only by the reactivity of evaporite sediments). As a consequence, the calculations simply reflect initial perturbation of the system upon fluid recharge, without taking into account the influence of dissolved oxygen. Throughout the calculations described above, Fe^{2+}-bearing sulfates are produced in abundance, even at intermediate Fe^{2+}/Fe_{Total} ratios. However, there is little evidence for the presence of such phases in the Meridiani outcrop [13]. Hydrated varieties of $Fe^{2+}SO_4 \cdot nH_2O$ are sensitive to dissolution, dehydration and oxidation as are other mixed-valence Fe bearing sulfates produced in evaporation and diagenesis calculations discussed above [43,80]. As a result, such phases are commonly converted to more oxidized mineral species. For example, in areas on Earth affected by acid mine drainage, typical sequences of Fe-sulfate mineral paragenesis have been established. Commonly, the youngest mineral products (Fe^{2+}-bearing sulfates) are found in close contact with pyrite, the mineral from which they are derived. As a result of burial diagenesis and further oxidation reactions, a general sequence is observed that begins with Fe^{2+}-sulfate minerals, transitions to mixed-valence Fe-sulfates, Fe^{3+}-sulfates, and finally Fe^{3+}-oxides and oxyhydroxides [80,85]. While such relationships further complicate the Fe-sulfate chemistry and mineralogy present in the outcrop, the calculations presented in this study suggest that Fe^{2+}-bearing sulfates should be a component of initial evaporite assemblages given previous evaluations of levels of O_2 in the martian atmosphere and the resulting implications of exceedingly slow Fe^{2+}(aq) oxidation rates. A pre-diagenetic mineral assemblage consisting of dominantly ferric Fe-bearing components is unlikely under such conditions and therefore oxidation of ferrous Fe components must have been a crucial process during diagenesis. A complete investigation of evaporation and diagenesis at Meridiani Planum will therefore need to address the kinetics of Fe^{2+}(aq) oxidation and the resulting effects of the process on sulfate mineral stability in high ionic strength aqueous fluids.

6. Constraints on evaporite geochemistry at Meridiani Planum

Because acidic weathering fluids derived from martian basalt are typically rich in Mg, Fe, Ca, SiO_2 and SO_4, these components will comprise the majority of the evaporite mineralogy present at the martian surface. The behavior of Fe in evaporitic and diagenetic settings must therefore be well understood. The results discussed above result from the first application of modeling both Fe^{2+} and Fe^{3+} as discrete evaporitic components related to Mars. The application of the model to unique fluids derived in the laboratory from weathering synthetic martian basalt is particularly relevant to the interpretation of Meridiani Planum geochemistry.

The major mineralogical products resulting from evaporation modeling include Mg-sulfate (epsomite), Ca-sulfate (gypsum/anhydrite), Fe^{2+}-sulfate (melanterite) and Fe^{3+}-sulfate (jarosite). Variability in the resulting evaporite mineral assemblage is dependent on factors such as the basalt lithology being weathered, redox conditions, and pH of weathering.

The stability of resulting mineral assemblages upon contact with diagenetic fluids suggests that porosity, fluid composition and initial mineralogy are among the most important factors. The transformation of jarosite to goethite is one major diagenetic reaction that is thermodynamically favored in the modeling discussed above.

The evaporation and diagenesis results are consistent with several geochemical data obtained at Meridiani Planum. For example, Mg-sulfates are likely an important component of the evaporite mineralogy at Meridiani Planum from the general correlation of Mg with SO_3 in APXS data obtained from the outcrop [15,16]. The formation of gypsum in all calculations is also consistent with mass balance calculations suggesting that Ca-sulfates are present in the outcrop [16,17]. Ferrous iron-bearing sulfates are predicted to be an important component of initial evaporite mineralogy, given the slow rate of Fe(II) oxidation expected under such conditions. The lack of observable ferrous iron-bearing sulfates suggests either that these phases never

formed, or that they were oxidized or dissolved, providing several possible mechanisms for ferric sulfate and Fe-oxide mineral formation. The requirement of acidic olivine weathering to produce the observed abundances of Mg-sulfates also requires the liberation of significant Fe^{2+} and SiO_2(aq). Therefore, these components played a significant role in the geochemical evolution of Meridiani outcrop material, likely in the form of ferrous sulfates and siliceous alteration phases.

The prediction of jarosite formation and subsequent alteration to goethite provides one mechanism by which hematite may have formed during diagenesis. Equilibrium between goethite and jarosite may have been reached and because goethite precipitated from Fe-rich acid sulfate solutions is usually poorly crystalline, hematite nodules may have initially formed by coagulation of poorly crystalline goethite. In addition, diagenesis results also show that alteration of an evaporite assemblage by a dilute fluid can result in the preservation of many soluble components. The overall product after specific diagenesis calculations (e.g., Fig. 14) bears a close resemblance to the evaporite portion of the Meridiani outcrop in light of all available data. The diagenesis calculations also place constraints on the nature of the phase which may have occupied the crystal-shaped molds. Gypsum is unlikely to be the phase which was removed because of its insolubility in relation to other sulfate phases implied to be present in the outcrop. Significant fluid flushing and transport would be required to remove gypsum. It is likely that the material which occupied the crystal-shaped molds was quite soluble if it was removed by simple dissolution (see [16,17]). For example, Clark et al. [16] suggest Mg–Cl phases could be suitable candidates and these phases are extremely soluble. As an alternative, the prediction of ferrous sulfates in this model provides another possible diagenetic reaction responsible for crystal-shaped mold formation. Such mineral phases could be removed by a combination of oxidation and dissolution, a process which would likely have little effect on the remaining evaporite portion of the outcrop.

Overall, the cyclic nature of evaporative processes envisaged for Meridiani Planum has likely been a controlling kinetic factor in many of the reactions discussed above. If aqueous events were cut off by evaporation, then some chemical processes may not have had adequate time to reach equilibrium. For example, sustenance of an acidic environment evolving from a basaltic substrate may have been controlled by this process. If acidic pH levels were not buffered by basaltic weathering before evaporation and precipitation of acidic salts, subsequent aqueous events would have continued to evolve down an acidic pathway because of several acid-generating reactions encountered upon dissolution of such phases. Decreasing buffering capacity (or reactivity) of the basalt after repeated periods of weathering likely contributed to this process. Fe redox disequilibrium is expected during evaporation as a result of competition between low Fe^{2+}(aq) oxidation rates and evaporating fluids. Aqueous Fe^{2+} was oxidized nevertheless, but the majority of oxidation is likely to have taken place during diagenesis. Potential oxidants of Fe^{2+}(aq) include atmospheric oxygen (notoriously slow at acidic pH) and UV photons (limited to near-surface waters).

In conclusion, the modeling results discussed above provide a foundation for understanding evaporite formation in exclusively basaltic environments. The knowledge of evaporite formation produced from simple weathering fluid evaporation enables more complicated processes typical of terrestrial environments to be understood. More importantly, while just one of several possibilities, a simple scenario has been found to be consistent with much of the available data related to Meridiani outcrop. This scenario first involves evaporation of an acidic, somewhat oxidized basaltic weathering fluid produced from weathering an olivine-bearing basalt. Subsequent recharge of a relatively dilute fluid into the resulting evaporite sediments drives the jarosite–goethite transformation reaction while preserving much of the initial soluble evaporite component.

Acknowledgements

We would like to thank the MER science and engineering teams for making this experience a truly unforgettable one. It has been a privilege and a pleasure to work with so many extraordinary individuals. NJT would like to thank Andrew Felmy, Richard Reeder and Martin Schoonen for helpful discussions and to Franco Frau for kindly granting use of his unpublished data. The authors would also like to thank D. Kirk Nordstrom, Giles M. Marion and an anonymous reviewer for thorough and insightful reviews. The MER project is funded by the National Aeronautics and Space Administration. This work was also partially supported by NASA Cosmochemistry Program grant NAG5-12916 to S.M.M.

Appendix A. Supplementary data

Supplementary data associated with this article can be found, in the online version, at doi:10.1016/j.epsl.2005.09.042.

References

[1] S.W. Squyres, J.P. Grotzinger, R.E. Arvidson, J.F. Bell III, P.R. Christensen, B.C. Clark, J.A. Crisp, W. Farrand, K.E. Herkenhoff, J.R. Johnson, G. Klingelhöfer, A.H. Knoll, S.M. McLennan, H.Y. McSween, R.V. Morris, J.W. Rice, R. Rieder, L.A. Soderblom, In-situ evidence for an ancient aqueous environment at Meridiani Planum, Mars, Science 306 (2004) 1709.

[2] R.E. Arvidson, F. Poulet, J.-P. Bibring, M. Wolff, A. Gendrin, R.V. Morris, J.J. Freeman, Y. Langevin, N. Mangold, G. Bellucci, Spectral reflectance and morphologic correlations in eastern Terra Meridiani, Mars, Science 307 (2005) 1591–1594.

[3] B.M. Hynek, Implications for hydrologic processes on Mars from extensive bedrock outcrops throughout Terra Meridiani, Nature 431 (2004) 156–159.

[4] L.A. Hardie, On the significance of evaporites, Annu. Rev. Earth Planet. Sci. 19 (1991) 131–168.

[5] D. Fernandez-Remolar, R.V. Morris, J.E. Gruener, R. Amils, A.H. Knoll, The Rio Tinto Basin, Spain: mineralogy, sedimentary geobiology, and implications for interpretation of outcrop rocks at Meridiani Planum, Mars, Earth and Planetary Science Letters 240 (2005) 149–167, doi:10.1016/j.epsl.2005.09.043.

[6] R.V. Morris, D.W. Ming, T.G. Graff, R.E. Arvidson, J.F. Bell III, S.A. Mertzman, J.E. Gruener, D.C. Golden, L. Le, G.A. Robinson, A terrestrial analogue for hematite spherules and sulfate in the Burns Formation at Meridiani Planum, Mars, Earth and Planetary Science Letters 240 (2005) 168–178, doi:10.1016/j.epsl.2005.09.044.

[7] C. Ptacek, D. Blowes, Predicting sulfate–mineral solubility in concentrated waters, in: C.N. Alpers, J.L. Jambor, D.K. Nordstrom (Eds.), Sulfate Minerals: Crystallography, Geochemistry and Environmental Significance, Reviews in Mineralogy and Geochemistry, 40, Mineralogical Society of America, Washington, D.C., 2000.

[8] R.T. Pabalan, K.S. Pitzer, Mineral solubilities in electrolyte solutions, in: K.S. Pitzer (Ed.), Activity Coefficients in Electrolyte Solutions, CRC Press, Boca Raton, 1991, pp. 435–490.

[9] K.S. Pitzer, Ion interaction approach: theory and data correlation, in: K.S. Pitzer (Ed.), Activity Coefficients in Electrolyte Solutions, CRC Press, Boca Raton, 1991, pp. 75–154.

[10] D.K. Nordstrom, Aqueous redox chemistry and the behavior of iron in acid mine waters, in: R.T. Wilkin, R.D. Ludwig, R.G. Ford (Eds.), Workshop on Monitoring Oxidation–Reduction Processes for Ground-Water Restoration, 2002, Dallas, TX.

[11] E.J. Reardon, R.D. Beckie, Modelling chemical equilibria of acid mine drainage: the $FeSO_4$–H_2SO_4–H_2O system, Geochim. Cosmochim. Acta 51 (1987) 2355–2368.

[12] C.J. Ptacek, D.W. Blowes, Geochemistry of concentrated waters at mine-waste sites, in: J.L. Jambor, D.W. Blowes, A.I.M. Ritchie (Eds.), Environmental Aspects of Mine Wastes, Short Course Series, vol. 31, Mineralogical Association of Canada, Vancouver, 2003, pp. 239–252.

[13] G. Klingelhöfer, R.V. Morris, B. Bernhardt, C. Schroeder, D.S. Rodionov, P.A. de Souza, A. Yen, R. Gellert, E.N. Evlanov, B. Zubkov, J. Foh, E. Kankeleit, P. Gutlich, D.W. Ming, F. Renz, T. Wdowiak, S.W. Squyres, R.E. Arvidson, Jarosite and hematite at Meridiani Planum from opportunity's Mossbauer spectrometer, Science 306 (2004) 1740.

[14] L.A. Soderblom, R.C. Anderson, R.E. Arvidson, J.F. Bell III, N.A. Cabrol, W. Calvin, P.R. Christensen, B.C. Clark, T. Economou, B.L. Ehlmann, W. Farrand, D. Fike, R. Gellert, T.D. Glotch, M. Golombek, R. Greeley, J. Grotzinger, K.E. Herkenhoff, D.J. Jerolmack, J.R. Johnson, B.L. Jolliff, G. Klingelhöfer, A. Knoll, Z.A. Learner, R. Li, M.C. Malin, S.M. McLennan, H.Y. McSween, D.W. Ming, R.V. Morris, J.W. Rice, L. Richter, R. Rieder, M. Sims, D. Rodionov, C. Schroeder, F. Seelos, J. Soderblom, S.W. Squyres, R. Sullivan, W.A. Watters, C. Weitz, M.B. Wyatt, A. Yen, J. Zipfel, Soils of eagle crater and Meridiani Planum at the opportunity rover landing site, Science 306 (2004) 1723.

[15] R. Rieder, R. Gellert, R.C. Anderson, J. Bruckner, B.C. Clark, G. Dreibus, T. Economou, G. Klingelhöfer, G.W. Lugmair, D.W. Ming, S.W. Squyres, C. d'Uston, H. Wanke, A. Yen, J. Zipfel, Chemistry of rocks and soils at Meridiani Planum from the alpha particle X-ray Spectrometer, Science 306 (2004) 1746.

[16] B.C. Clark, S.M. McLennan, R.V. Morris, R. Gellert, B.L. Jolliff, A.H. Knoll, T.K. Lowenstein, D.W. Ming, N.J. Tosca, P.R. Christensen, S. Gorevan, A. Yen, J. Bruckner, W. Calvin, G. Dreibus, W. Farrand, G. Klingelhöfer, H. Wanke, J. Zipfel, J.F. Bell III, S.W. Squyres, J. Grotzinger, H.Y. McSween, R. Rieder, K.E. Herkenhoff, Chemistry and mineralogy of outcrops at Meridiani Planum, Earth and Planetary Science Letters 240 (2005) 73–94, doi:10.1016/j.epsl.2005.09.040.

[17] S.M. McLennan, J.F. Bell III, W.M. Calvin, P.R. Christensen, B.C. Clark, P.A. de Souza, J. Farmer, W. Farrand, D. Fike, R. Gellert, A. Ghosh, T. Glotch, J.P. Grotzinger, B.C. Hahn, K.E. Herkenhoff, J.A. Hurowitz, J.R. Johnson, S.S. Johnson, B.L. Jolliff, G. Klingelhöfer, A.H. Knoll, Z.A. Learner, M.C. Malin, H.Y. McSween, J. Pocock, S.W. Ruff, L.A. Soderblom, S.W. Squyres, N.J. Tosca, W.A. Watters, M.B. Wyatt, A. Yen, Provenance and diagenesis of the evaporite-bearing Burns Formation, Meridiani Planum, Mars, Earth and Planetary Science Letters 240 (2005) 95–121, doi:10.1016/j.epsl.2005.09.041.

[18] R. Gellert, R. Rieder, R.C. Anderson, J. Bruckner, B.C. Clark, G. Dreibus, T. Economou, G. Klingelhöfer, G.W. Lugmair, D.W. Ming, S.W. Squyres, C. d'Uston, H. Wanke, A. Yen, J. Zipfel, Chemistry of rocks and soils in Gusev from alpha particle X-ray spectrometer, Science 305 (2004) 829–832.

[19] J.P. Grotzinger, J.F. Bell III, W. Calvin, B.C. Clark, D.A. Fike, M. Golombek, R. Greeley, K.E. Herkenhoff, B.L. Jolliff, A.H. Knoll, M.C. Malin, S.M. McLennan, T. Parker, L. Soderblom, J.N. Sohl-Dickstein, S.W. Squyres, N.J. Tosca, W.A. Watters, Stratigraphy, sedimentology, and depositional environment of the Burns Formation, Meridiani Planum, Mars, Earth and Planetary Science Letters 240 (2005) 11–72, doi:10.1016/j.epsl.2005.09.039.

[20] J.A. Rard, R.F. Platford, Experimental methods: isopiestic, in: K.S. Pitzer (Ed.), Activity Coefficients in Electrolyte Solutions, CRC Press, Boca Raton, 1991, pp. 209–278.

[21] J.N. Butler, R.N. Roy, Experimental methods: potentiometric, in: K.S. Pitzer (Ed.), Activity Coefficients in Electrolyte Solutions, CRC Press, Boca Raton, 1991, pp. 155–208.

[22] C.E. Harvie, N. Moller, J.H. Weare, The prediction of mineral solubilities in natural waters: the Na–K–Mg–Ca–H–Cl–SO_4–OH–HCO_3–CO_3–CO_2–H_2O system to high ionic strengths at 25 °C, Geochim. Cosmochim. Acta 48 (1984) 723–751.

[23] A.G. Fairen, D. Fernandez-Remolar, J.M. Dohm, V.R. Baker, R. Amils, Inhibition of carbonate synthesis in acidic oceans on early Mars, Nature 431 (2004) 423–426.
[24] G.M. Marion, D.C. Catling, J.S. Kargel, Modeling aqueous ferrous iron chemistry at low temperatures with application to Mars, Geochim. Cosmochim. Acta 67 (2003) 4251–4266.
[25] C. Christov, Pitzer ion-interaction parameters for Fe(II) and Fe(III) in the quinary {Na+K+Mg+Cl+SO_4+H_2O} system at T=298.15 K, J. Chem. Thermodyn. 36 (2004) 223–235.
[26] E.J. Reardon, Ion interaction parameters for $AlSO_4$ and application to the prediction of metal sulfate solubility in binary salt systems, J. Phys. Chem. 92 (1988) 6426–6431.
[27] C. Christov, Thermodynamic study of the K–Mg–Al–Cl–SO_4–H_2O system at the temperature 298.15 K, Calphad 25 (3) (2001) 445–454.
[28] C. Christov, Thermodynamic study of Quaternary systems with participation of ammonium and sodium alums and chromium alums, Calphad 26 (3) (2002) 341–352.
[29] J.M. Delany, S.R. Lundeen, The LLNL thermochemical database (1990) 150.
[30] V.B. Parker, I.L. Khodakovskii, Thermodynamic properties of the aqueous ions (2+ and 3+) of iron and the key compounds of iron, J. Phys. Chem. Ref. Data 24 (5) (1995) 1699–1745.
[31] J.W. Johnson, E.H. Oelkers, H.C. Helgeson, SUPCRT92: a software package for calculating the standard molal thermodynamic properties of minerals, gases, aqueous species, and reactions from 1 to 5000 bar and 0 to 1000 deg C, Comput. Geosci. 18 (1992) 899–947.
[32] E.L. Shock, H.C. Helgeson, Calculation of the thermodynamic and transport properties of aqueous species at high pressures and temperatures: correlation algorithms for ionic species and equation of state predictions to 5 kb and 1000 deg C, Geochim. Cosmochim. Acta 52 (1988) 2009–2036.
[33] B.S. Hemingway, R.R. Seal, I.-M. Chou, Thermodynamic data for modeling acid mine drainage problems: compilation and estimation of data for selected soluble iron–sulfate minerals, United States Geological Survey Open File Report 02-161, 2002.
[34] J. Majzlan, A. Navrotsky, U. Schwertmann, Thermodynamics of iron oxides: Part III. Enthalpies of formation and stability of ferrihydrite (~$Fe(OH)_3$), schwertmannite (~$FeO(OH)_{3/4}(SO_4)_{1/8}$), and ε-Fe_2O_3, Geochim. Cosmochim. Acta 68 (5) (2004) 1049–1059.
[35] L.B. Pankratz, W.W. Weller, Thermodynamic data for ferric sulfate and indium sulfate, U.S. Bur. Mines Rep. (1969).
[36] R.A. Robie, B.S. Hemingway, J.R. Fisher, Thermodynamic properties of minerals and related substances at 298.15 K and 1 bar (10^5 Pascals) pressure and at higher temperatures, U. S. Geol. Surv. Bull. 1452 (1979) 1456.
[37] H.C. Helgeson, J.M. Delany, H.W. Nesbitt, D.K. Bird, Summary and critique of the thermodynamic properties of rock-forming minerals, Am. J. Sci. 278a (1978) 229.
[38] C. Drouet, A. Navrotsky, Synthesis, characterization, and thermochemistry of K–Na–H_3O jarosites, Geochim. Cosmochim. Acta 67 (11) (2003) 2063–2076.
[39] J.W. Larson, P. Cerutti, H.K. Garber, L.G. Helper, Electrode potentials and thermodynamic data for aqueous ions. Copper, zinc, cadmium, iron, cobalt, and nickel, J. Phys. Chem. 72 (1968) 2902–2907.
[40] C.M. Bethke, The Geochemist's Workbench, Release 4.0: A User's Guide to Rxn, Act2, Tact, React, and Gtplot, University of Illinois, 2002, 224 pp.
[41] L.N. Plummer, D.L. Parkhurst, G.W. Fleming, S.A. Dunkle, A computer program incorporating Pitzer's equations for calculation of geochemical reactions in brines, United States Geological Survey Water-Resources Investigation Report 88-4153, 1988, p. 310.
[42] C.M. Bethke, Geochemical Reaction Modeling, Oxford, New York, 1996, 397 pp.
[43] F. Frau, The formation–dissolution–precipitation cycle of melanterite at the abandoned pyrite mine of Genna Luas in Sardinia, Italy: environmental applications, Mineral. Mag. 64 (6) (2000) 995–1006.
[44] D.K. Nordstrom, J.L. Munoz, Geochemical Thermodynamics, Blackwell, Boston, 1994, 493 pp.
[45] D.K. Nordstrom, E.A. Jenne, J.W. Ball, Redox equilibria of iron in acid mine waters, in: E.A. Jenne (Ed.), Chemical Modeling in Aqueous Systems, American Chemical Society, Washington, D.C., 1979, pp. 51–79 (93).
[46] D.K. Nordstrom, Trace metal speciation in natural waters: computational vs. analytical, Water Air Soil Pollut. 90 (1996) 257–267.
[47] C.N. Alpers, D.K. Nordstrom, Geochemical modeling of water–rock interactions in mining environments, in: G.S. Plumlee, M.J. Logsdon (Eds.), The Environmental Geochemistry of Mineral Deposits: Part A. Processes, Techniques, and Health Issues, Reviews in Economic Geology, vol. 6A, Society of Economic Geologists, Littleton, CO, 1999, pp. 289–323.
[48] D.K. Nordstrom, Modeling of low-temperature geochemical processes, in: H.D. Holland, K.K. Turekian (Eds.), Treatise on Geochemistry, Elsevier, 2003, pp. 37–72 5.
[49] T.K. Lowenstein, M.N. Timofeeff, S.T. Brennan, L.A. Hardie, R.V. Demicco, Oscillations in Phanerozoic seawater chemistry: evidence from fluid inclusions, Science 294 (2001) 1086–1088.
[50] M.N. Timofeeff, T.K. Lowenstein, S.T. Brennan, R.V. Demicco, H. Zimmermann, J. Horita, L.E. von Borstel, Evaluating seawater chemistry from fluid inclusions in halite: examples from modern marine and nonmarine environments, Geochim. Cosmochim. Acta 65 (14) (2001) 2293–2300.
[51] N.J. Tosca, S.M. McLennan, D.H. Lindsley, M.A.A. Schoonen, Acid-sulfate weathering of synthetic Martian basalt: the acid fog model revisited, J. Geophys. Res. 109 (E05003) (2004), doi:10.1029/2003JE002218.
[52] S.R. Taylor, S.M. McLennan, The Continental Crust: Its Composition and Evolution, Blackwell, Oxford, 1985, 312 pp.
[53] R.J. Spencer, L.A. Hardie, Control of seawater composition by mixing of river waters and mid-ocean ridge hydrothermal brines, in: R.J. Spencer, I.-M. Chou (Eds.), Fluid–Mineral Interactions: A Tribute to H.P. Eugster, Geochemical Society Special Publication, vol. 2, Geochemical Society, 1990, pp. 409–419.
[54] J.-P. Bibring, Y. Langevin, A. Gendrin, B. Gondet, F. Poulet, M. Berthe, A. Soufflot, R.E. Arvidson, N. Mangold, J.F. Mustard, P. Drossart, O. Team, Mars surface diversity as revealed by the OMEGA/Mars express observations, Science 307 (2005) 1576–1581.
[55] A. Gendrin, N. Mangold, J.-P. Bibring, Y. Langevin, B. Gondet, F. Poulet, G. Bonello, C. Quantin, J.F. Mustard, R.E. Arvidson, S. LeMouelic, Sulfates in Martian layererd terrains: the OMEGA/Mars express view, Science 307 (2005) 1587–1591.
[56] Y. Langevin, F. Poulet, J.-P. Bibring, B. Gondet, Sulfates in the north polar region of Mars detected by OMEGA/Mars Express, Science 307 (2005) 1584–1586.
[57] M.D. Lane, M.D. Dyar, J.L. Bishop, Spectroscopic evidence for hydrous iron sulfate in the Martian soil, Geophys. Res. Lett. 31 (L19702) (2004), doi:10.1029/2004GL021231.

[58] H.Y. McSween, K. Keil, Mixing relationships in the Martian regolith and the composition of globally homogeneous dust, Geochim. Cosmochim. Acta 64 (12) (2000) 2155–2166.
[59] S.M. McLennan, Chemical composition of Martian soil and rocks: complex mixing and sedimentary transport, Geophys. Res. Lett. 27 (9) (2000) 1335–1338.
[60] D.W. Ming, R.V. Morris, R. Gellert, A. Yen, J.F. Bell III, D. Blaney, P.R. Christensen, L. Crumpler, P. Chu, W.H. Farrand, S. Gorevan, K.E. Herkenhoff, G. Klingelhöfer, R. Rieder, D. Rodionov, S.W. Ruff, C. Schroeder, S.W. Squyres, Geochemical and mineralogical indicators for aqueous processes on the West Spur of the Columbia Hills in Gusev Crater, Lunar and Planetary Science XXXVI, Abstract #2125, Lunar and Planetary Institute, Houston, 2005, CD-ROM.
[61] A. Wang, L.A. Haskin, S.W. Squyres, R.E. Arvidson, L. Crumpler, R. Gellert, J.A. Hurowitz, C. Schroeder, N.J. Tosca, K.E. Herkenhoff, B.L. Jolliff, Sulfate deposition in regolith exposed in trenches on the plains between the Spirit landing site and Columbia Hills in Gusev Crater, Mars, Lunar and Planetary Science XXXVI, Abstract #2236, Lunar and Planetary Institute, Houston, 2005, CD-ROM.
[62] J.A. Hurowitz, S.M. McLennan, N.J. Tosca, R.E. Arvidson, J. Michalski, D.W. Ming, C. Schroeder, S.W. Squyres, In-Situ and experimental evidence for acidic weathering of rocks and soils on Mars, J. Geophys. Res., in press.
[63] P.C. Singer, W. Stumm, Acid mine drainage—the rate determining step, Science 167 (3921) (1970) 1121–1123.
[64] F.J. Millero, S. Sotolongo, M. Izaguirre, The oxidation kinetics of Fe(II) in seawater, Geochim. Cosmochim. Acta 51 (1987) 793–801.
[65] R.G. Burns, Rates and mechanisms of chemical weathering of ferromagnesian silicate minerals on Mars, Geochim. Cosmochim. Acta 57 (19) (1993) 4555–4574.
[66] D.C. Catling, J.M. Moore, The nature of coarse-grained crystalline hematite and its implications for the early environment of Mars, Icarus 165 (2003) 277–300.
[67] M.W. Schaefer, Are there abiotically-precipitated iron formations on Mars?, in: M.D. Dyar, C. McCammon, M.W. Schaefer (Eds.), Mineral Spectroscopy: A Tribute to Roger G. Burns, Geochemical Society Special Publication, vol. 5, The Geochemical Society, Houston, 1996, pp. 381–393.
[68] D.K. Nordstrom, C.N. Alpers, Geochemistry of acid mine waters, in: G.S. Plumlee, M.J. Logsdon (Eds.), The Environmental Geochemistry of Mineral Deposits: Part A. Processes, Techniques, and Health Issues, Society of Economic Geologists, Inc., Littleton, 1999.
[69] D.O. Whittemore, D. Langmuir, Ferric oxyhydroxide microparticles in water, Environ. Health Perspect. 9 (1974) 173–176.
[70] D. Langmuir, Particle size effect on the reaction goethite=hematite+water, Am. J. Sci. 271 (1971) 147–156.
[71] D. Langmuir, D.O. Whittemore, Variations in the stability of precipitated ferric oxyhydroxides, Non-Equilibrium Systems in Natural Water Chemistry, Advances in Chemistry Series, vol. 106, American Chemical Society, Washington, D.C., 1971, p. 209.
[72] J.M. Bigham, U. Schwertmann, S.J. Traina, R.L. Winland, M. Wolf, Schwertmannite and the chemical modeling of iron in acid sulfate waters, Geochim. Cosmochim. Acta 60 (12) (1996) 2111–2121.
[73] J.M. Bigham, D.K. Nordstrom, Iron and aluminum hydroxysulfates from acid sulfate waters, in: C.N. Alpers, J.L. Jambor, D.K. Nordstrom (Eds.), Sulfate Minerals: Crystallography, Geochemistry and Environmental Significance, Reviews in Mineralogy and Geochemistry, vol. 40, Mineralogical Society of America, Washington, D.C., 2000.
[74] J. Jonsson, P. Persson, S. Sjoberg, L. Lovgren, Schwertmannite precipitated from acid mine drainage: phase transformation, sulphate release and surface properties, Appl. Geochem. 20 (2005) 179–191.
[75] J.L. Jambor, J.E. Dutrizac, Occurrence and constitution of natural and synthetic ferrihydrite, a widespread iron oxyhydroxide, Chem. Rev. 98 (1998) 2549–2585.
[76] C.N. Alpers, D.K. Nordstrom, J.W. Ball, Solubility of jarosite solid solutions precipitated from acid mine waters, Iron Mountain, California, USA, Sciences Geologique, Bulletin 42 (4) (1989) 281–298.
[77] L.H. Filipek, D.K. Nordstrom, W.H. Ficklin, Interaction of acid mine drainage with waters and sediments of West Squaw Creek in the West Shasta Mining District, California, Environ. Sci. Technol. 21 (1987) 388–396.
[78] D.T. Long, N.E. Fegan, J.D. McKee, W.B. Lyons, M.E. Hines, P.G. Macumber, Formation of alunite, jarosite and hydrous iron oxides in a hypersaline system: Lake Tyrell, Victoria, Australia, Chem. Geol. 96 (1992) 183–202.
[79] R.V. Morris, T. Graff, M.D. Lane, D.C. Golden, C.S. Schwandt, T.D. Shelfer, D.W. Ming, S.A. Mertzman, J.F. Bell III, J. Crisp, P.R. Christensen, Acid sulfate alteration products of a tholeiitic basalt: implications for interpretation of Martian thermal emission spectra, Lunar and Planetary Science XXXI, Abstract 2014, 2000, Houston (CD-ROM).
[80] J.L. Jambor, D.K. Nordstrom, C.N. Alpers, Metal-sulfate salts from sulfide mineral oxidation, in: C.N. Alpers, J.L. Jambor, D.K. Nordstrom (Eds.), Sulfate Minerals: Crystallography, Geochemistry and Environmental Significance, Reviews in Mineralogy and Geochemistry, vol. 40, Mineralogical Society of America, Washington, D.C., 2000.
[81] P. Buurman, In vitro weathering products of pyrite, Geol. Mijnb. 54 (1) (1975) 101–105.
[82] T. Buckby, S. Black, M.L. Coleman, M.E. Hodson, Fe-sulphate-rich evaporative mineral precipitates from the Rio Tinto, southwest Spain, Mineral. Mag. 67 (2) (2003) 263–278.
[83] R.M. Garrels, F.T. Mackenzie, Origin of the chemical compositions of some springs and lakes, in: W. Stumm (Ed.), Equilibrium Concepts in Natural Water Systems, Advances in Chemistry Series, vol. 67, American Chemical Society, Washington, D.C., 1967, pp. 222–242.
[84] D.K. Nordstrom, C.N. Alpers, C.J. Ptacek, D.W. Blowes, Negative pH and extremely acidic mine waters from Iron Mountain, California, Environ. Sci. Technol. 34 (2000) 254–258.
[85] J.K. Jertz, J.D. Rimstidt, Efflorescent iron sulfate minerals: paragenesis, relative stability, and environmental impact, Am. Mineral. 88 (2003) 1919–1932.